NASA Contractor Report 185168

Conceptual Design of a Moving Belt Radiator Shuttle-Attached Experiment

Technical Requirements Document

Jerry L. Aguilar
Arthur D. Little, Inc.

November 1989

Prepared for
Lewis Research Center
Under Contract NAS3-25356

NASA
National Aeronautics and
Space Administration

NASA Contractor Report 185168

Conceptual Design of a Moving Belt Radiator Shuttle-Attached Experiment

Technical Requirements Document

Jerry L. Aguilar
Arthur D. Little, Inc.

November 1989

Prepared for
Lewis Research Center
Under Contract NAS3-25356

NASA
National Aeronautics and
Space Administration

Arthur D Little

TABLE OF CONTENTS

1.0 SUMMARY

This document describes a proposed experiment which will demonstrate the dynamic and thermal characteristics of a Moving Belt Radiator. This type of radiator, along with the Liquid Droplet and Rotating Bubble Membrane Radiators, are classified as advanced concepts currently under development. The Moving Belt Radiator is predicted to have a weight one fifth to one third that of the current baseline heat pipe system in addition to higher survivability, options for retraction, better maneuverability, and extremely high heat rejection levels (5 to 200 MW). This level of heat rejection would permit many missions and technologies currently being considered. These would include use of nuclear power in space, Mars transfer mission, manned space platforms, and burst power systems.

The moving belt radiator system is one in which the waste energy from a spacecraft, space station, or satellite, is transported to the belt (a closed hoop) via an interface heat exchanger. In this heat exchanger, a fluid bath provides a direct path for the energy to transfer to the belt. The belt is drawn through the bath and then exposed to space, where the energy is radiated out. Various concepts have been considered for the belt, including a mesh structure in which fluid menisci are formed on the belt and become the radiating surface, and a belt which encases a phase change material storing the thermal energy. The shape of all belts is assumed to be the same, a cylindrical hoop. The shape is attained through the use of centrifugal forces of a rotating belt, i.e. with no other forces dominating, the centrifugal forces will cause the belt to stretch until a taut hoop is formed. The speed and material properties will determine how stiff a hoop is ultimately formed.

Arthur D. Little, Inc. has been developing the Moving Belt Radiator concept with the NASA Lewis Research Center. During the past few years various studies and laboratory experiments have been conducted at Arthur D. Little. These include dynamic analysis and testing, heat exchanger sealing, measurement of candidate belt material properties, and wettability testing of candidate working fluids.

The most recent experiment was a test of the dynamic characteristics aboard the NASA KC-135 research aircraft in which it was demonstrated that, in a reduced gravity environment, the belt would form a hoop under certain conditions. Also, it was shown that the belt would form a hoop after being deployed from a stowed configuration, and that after a perturbation the belt would deform and then return to the original shape. One more series of flights is scheduled for early 1990, in which new belt materials will be tested. Further experimentation is required with larger belts and in an environment free from air currents, KC-135 vibrations, and variable gravity levels. Thermal testing must also be included. The thermal testing could be accomplished in vacuum chambers but the dynamic testing requires a space based platform. The KC-135 cannot accommodate larger belts than have already been tested and no simultaneous dynamic and thermal testing is possible unless a large vacuum chamber is installed in the KC-135. It is therefore necessary to develop a shuttle flight experiment which would allow an integrated test to be conducted.

The primary focus of the space flight experiment should be the verification of dynamic characteristics. A thermal test could be integrated into the apparatus such that a working version of a Moving Belt Radiator could be demonstrated. An added feature of the proposed experiment is that retraction of the belt would be demonstrated.

The belt would be between 2.4 m and 3.7 m (8 ft. and 12 ft.) diameter, which is at least twice the size of the article tested on the KC-135. The physical integration of the experiment into a shuttle payload would be relatively straightforward. The experiment would be located on the Hitchhiker-M carrier in the shuttle bay.

The requirements for an experiment of this type would include a minimum of two hours of testing, orienting the shuttle bay away from the sun for thermal testing, and approximately 1500 W of power. The required supervision would be minimal and no extravehicular activity or remote manipulator system use would be necessary.

2.0 INTRODUCTION

2.1 BACKGROUND

As part of ongoing work with NASA Lewis Research Center since 1982, Arthur D. Little, Inc. (ADL) has been developing the Moving Belt Radiator (MBR) concept for use on spacecraft. In this concept, shown in Figure 1, a belt is drawn through an interface heat exchanger (IHX) containing a low vapor pressure working fluid which functions as the heat sink for the power generation or environmental conditioning system. The moving belt passes through the IHX where it is heated by the hot fluid; then as the belt travels through space it radiates the energy to the background environment. This effort initially focussed on liquid belt radiators (LBR) wherein a meniscus of the IHX fluid formed on a mesh structure, the belt. This concept resulted in excellent heat transfer characteristics in the IHX and could take advantage of the heat of fusion of the IHX liquid (tin, lithium, etc.). Recently, increased attention has been focussed on a unique hybrid belt radiator (HBR) design which retains the excellent heat transfer characteristics of the LBR in the IHX but does not result in a free liquid surface exposed to space.

This work, described in References 1 - 3, shows that appropriate MBR configurations have major advantages for use in space missions with substantial heat rejection requirements including:

- An ability to stow 200 MW radiators in the shuttle bay;
- Relatively simple deployment from a stowed position;
- Weight of one fifth to one third that of heat pipe or pumped fluid configurations;
- Favorable survivability characteristics against both natural environment and hostile threats.

These attributes could both enhance and enable future NASA and Department of Defense (DOD) missions as their thermal heat rejection needs increase over the coming decades.

In order to verify the basic dynamic characteristics of a MBR, a 1.2 m (4 ft.) belt was tested aboard the KC-135 test bed in April of 1989. This test only addressed the dynamics of the belt with no testing of the heat transfer system. The data that was collected is primarily in the form of video and 16 mm film. Preliminary results confirm that some belts do form a cylindrical shape in a reduced

gravity environment when driven in a circular fashion. Further investigation will be conducted in order to determine why some belts did not form cylindrical shapes. From this series of tests, the major characteristics demonstrated were:

- Belts made from the proper material and thickness will form a hoop;
- Belts, when stowed, can be deployed and will assume a cylindrical shape;
- Belts which are not moving can be started in reduced gravity and will form a hoop.

A second series of KC-135 tests is scheduled for early in 1990. This second series of tests will endeavor to provide more data on specific belt characteristics which are favorable to MBR applications.

2.2 JUSTIFICATION FOR SPACE SHUTTLE TESTING

This document describes the essential features of a space flight experiment which can verify essential dynamic and thermal characteristics of a MBR system during deployment and operation, thereby allowing for refinement of the analytical projections of the overall MBR performance. A comparison of MBR performance with alternative radiator concepts can then be performed for advanced missions having substantial heat rejection requirements.

A small scale MBR has been tested on two KC-135 flights in April 1989. On these KC-135 flights reduced-g can be achieved for approximately 20 seconds. For small and relatively stiff belts, verification of the dynamic characteristics can be accomplished on the KC-135. If larger and more flexible belts are to be tested, then extended time in reduced-g is required. This can only be achieved in a space flight experiment. Also, this experiment will provide an environment in which to test the dynamics with no influence from earth's atmosphere, i.e. no air induced perturbations. As with any thin and flexible material, an air gust could influence the shape of the belt. In a KC-135 flight, the actual period of reduced-g varies from parabola to parabola. During the 20 second parabola, a reduced gravity environment of varying g-level is provided. The gravity field can vary from +0.1 g to -0.1 g. Past dynamic analysis of belts has predicted that these acceleration levels can be too high for some belts, which was evident in the first series of KC-135 flights.

One of the key issues now requiring resolution as part of an overall program is to verify experimentally, in a reduced-g environment, the dynamic characteristics during deployment and operation, thus providing a basis for comparison of these characteristics with analytical projections. Only limited information can be generated experimentally using ground based facilities for the required reduced-g test due to inherent time limitations imposed by such facilities (maximum of 20 seconds). Confirmation of dynamic characteristics will, therefore, require a larger test bed and longer term testing in a space environment.

The dynamic characteristics that should be examined during a space flight experiment are:

- Deployment to a cylindrical shape with no support structure;
- Required deployment time;
- Required time to damp out perturbations;
- Allowable acceleration levels;

- Retraction capability.

Additionally, a space flight experiment will allow the thermal characteristics to be tested in a space environment. The IHX will be filled with the working fluid and additional data will be gained from testing a working model of a MBR. The option to remove the working fluid from the experiment, thereby eliminating the thermal testing, can be exercised at any time. This document will, however, describe an experiment which will include the working fluid and thermal testing.

The thermal characteristics that will be examined in the space flight experiment are:

- The proposed sealing apparatus;
- The heat transfer characteristics;
- The vaporization rate of the working fluid.

The information gained in the KC-135 flights is a good base on which to build. The additional testing that can only be accomplished in a longer duration microgravity environment will be extremely valuable to the progress of MBR technology. The proposed shuttle experiment will, therefore, provide us with the ability to test a belt such that:

- No influence from air currents is present;
- KC-135 variable gravity levels are eliminated;
- Belt diameters between 2.4 and 3.7 meters (8 to 12 feet) are possible;
- A very flexible belt which requires more than 20 seconds to damp out perturbations can be examined;
- A complete working model of a MBR can be demonstrated.

2.3 DEPLOYMENT

Several modes of MBR deployment have been assessed and their impacts on stowability, deployment, and system weight evaluated. These include:

- Using lightweight, extendable, boom structures to establish the shape and movement of the belt.
- Taking advantage of the zero gravity environment and centrifugal forces such that the belt can self deploy into a hoop structure (Figure 1).

Previous work at ADL has indicated that both approaches result in attractive mechanical, thermal, and weight characteristics (Reference 1). The self deployed option, however, has the potential for very low weight by virtue of eliminating the need for structural deployment components. However, this option produces a complex dynamic system which must be analyzed and tested.

2.4 DYNAMIC ANALYSIS

The dynamics of the MBR are complex, particularly during deployment and when perturbed by short or long term acceleration fields. In recognition of this, ADL has developed a unique computer modeling program referred to as BERS, which allows for the dynamic analyses of such "floppy structures" as a function of their physical characteristics and imposed force fields. This model uses a lumped-parameter representation of the MBR structure. The formulation of the equations of motion and the interactions between the nodes are described in Appendix A. The results of this model indicate that:

- The equilibrium shape of the MBR structure is a hoop with the stiffness determined by belt materials, physical dimensions, and angular velocity.
- A short term physical disturbance, such as that resulting from a docking maneuver, should dampen out after a few belt revolutions. See Figure 2 for a sample plot of the projected shape during the short term acceleration.
- Under sustained acceleration fields the belt will elongate in shape and eventually become inoperative. The allowable duration of such accelerations will depend on the magnitude of the acceleration and the characteristics of the belt. See Figure 3 for a sample plot of the projected shape during an extended acceleration.
- Increased angular velocity increases stiffness and reduces susceptibility to gross deformation.

The experimental design will endeavor to allow verification of these characteristics.

2.5 THERMAL ANALYSIS

A parametric study of the thermal characteristics of possible MBR systems was performed and is covered extensively in References 1 and 2. Reference 3 details ground based thermal testing that was performed at ADL. Appendices B and C contain the development of the equations required to complete the parametric studies. Following is a brief description of the assumptions, procedures, and results of the thermal analysis.

Thermal characteristics were developed for all types of belt radiator systems, namely the LBR, HBR, and MBR. The calculation of radiation heat transfer characteristics are similar for all three systems, with a very important consideration being the view factor; Appendix B describes the development of the view factor equations.

The emissivities will vary with each type of belt system. The LBR, which has a liquid exposed to space, can have a relatively high emissivity if certain oils are used. Emissivities up to 0.8 can be achieved for moderate and low temperatures. For higher temperature applications, liquid metals are prime candidates for the working fluid. The drawback of liquid metals is that the emissivities are much lower, on the order of 0.1. With the HBR (phase change material encased in a belt) and the MBR (no liquid except in the IHX) the emissivity is a function of the belt material. With the

solid belt system the belt can be designed to be a near perfect black body (emissivity of 1.0). The higher the emissivity, the smaller the required area for a given heat load which is another advantage for this type of system. Practical emissivities would be in 0.8 to 1.0 range.

The equations and methodology used to analyze a belt system are described in Appendix C. Although the information in Appendix C was written specifically for the 75 kW point design study of Reference 2, the equations can be applied to any belt radiator system.

3.0 OBJECTIVES AND SCOPE

The overall objective of this program is to design a space flight experiment which would:

- Demonstrate that the belt radiator can be deployed from a stowed position and will assume the shape indicated in Figure 1 within a reduced-g environment;
- Measure belt dynamic response to low level acceleration fields and to impulse forces which might result from a docking maneuver or other sudden change in spacecraft position;
- Verify the computer dynamic models used to predict belt motion as a function of belt physical parameters, operating parameters, and spacecraft motion;
- Verify the predicted thermal characteristics of the MBR;
- Demonstrate retraction capabilities of a MBR system.

The flight experiment will be designed under conditions of belt speed, belt physical parameters, etc. which are consistent with those that would be used in full size working radiator systems. This is in contrast to the ground based reduced-g experiments where belt speeds and dimensions have to be adjusted to provide meaningful responses in the limited time periods allowed by the test facilities (2 to 25 seconds).

The flight experiment will be designed such that dimensions and belt dynamic characteristics are scaled equally. Some of the important items to be scaled are:

- Dimensions of the belt and IHX;
- Mass of belt and IHX;
- Damping properties of the system;
- Stiffness properties of the system.

The experimental apparatus will be designed to allow a high level of flexibility in the range of experiments to be conducted, i.e., to allow variation in operating conditions during the experiment. The experimental design and associated data acquisition will be consistent with safe operation on one of the space shuttle experimental test beds.

A functioning MBR will require a low vapor pressure liquid (gallium being the prime candidate) in the IHX. If no technical or safety issues preclude the use of an IHX liquid, then it would be desirable to include this capability in the experiment. Insight into the thermal characteristics would be gained as well as verification of seal performance in reduced-g and vacuum. A sealing system must be designed and tested in order to assure that no working fluid will contaminate any other experiment or the shuttle itself. Ground testing will be conducted in order to verify that the seals

will withstand the vibration, thermal, and vacuum environments that are present in low earth orbit and during shuttle ascent and decent. The sealing arrangement will allow for redundancy; in the event that one seal fails, a back-up will maintain overall integrity. The expected volume of working fluid is approximately one liter. The proposed ground tests include:

- Vacuum chamber tests;
- Vibration tests;
- Thermal shock tests.

The verification of the dynamic characteristics will be of prime importance and the thermal characteristics of secondary importance. The thermal testing can be eliminated from the design at any time without delaying the work on the MBR experiment. Also, the working fluid will be in a separate container and need never be introduced into the IHX if a possible danger arises during the flight.

4.0 RELATIONSHIP TO NASA MISSIONS

Many types of missions would potentially benefit from an MBR, such as NASA and DOD missions which require:

- Burst power: During low power consumption periods the MBR could dissipate any excess power.
- Storage of cryogenic fuels: Using an MBR system the cryogenic fuels could be maintained at very low temperatures.
- High maneuverability: The relative ease with which an MBR can be deployed allows high maneuverability missions to be considered. Two methods can be employed during maneuvers: retract the MBR and redeploy when the maneuver is completed; or limit the maneuver accelerations such that the belt will not fail.

For certain DOD missions, a large area conventional radiator would be an inviting target for hostile threats. The MBR may be less susceptible to such threats since puncture of the belt surface would not necessarily impair overall MBR operation.

The MBR has many of the weight and deployability attributes of the Liquid Droplet Radiator (LDR) also under development for similar applications. For this class of radiator, major weight and deployment advantages exist in applications such as:

- Orbital Transfer Vehicles (OTV) using a nuclear Brayton cycle power system to generate 10 MW of electric power;
- 100 kW nuclear Stirling engine power systems;
- Manned space platforms and growth versions of the space station;
- Laser platforms and particle beam vehicles;
- Space based radar;
- Mars transfer vehicle;
- Certain SP-100 and multimegawatt space power platforms.

Successful MBR development would, therefore, either enhance or enable a broad range of NASA and DOD missions. In particular, missions with relatively large heat rejection requirements (>200kW) can be enhanced significantly, particularly when the stowed volume of a heat pipe radiator system becomes substantial.

5.0 TECHNOLOGY BENEFITS

Although of simple design, the space flight experiment which will be developed during this program will have major benefits to the development of advanced radiator systems and to the broader issue of understanding the dynamic characteristics of "floppy" space structures. Specific benefits will include:

- Verification of critical elements of MBR dynamic characteristics, which will allow continued development of this concept with a high level of confidence that the constraints imposed by dynamic considerations are well understood;
- Refinement of dynamic models used to project the dynamic characteristics of MBR systems both in normal operational modes and when subjected to acceleration fields. These improved models will make it possible to design a more reliable and effective advanced radiator system and determine constraints on spacecraft motion;
- Improved understanding of the dynamic characteristics of the whole category of "floppy" structures. Understanding of the dynamics of these "floppy" structures will be required to implement a broad range of advanced radiator systems (LDR, etc.) and solar collector systems with large lightweight area requirements;
- Improved understanding of sealing specific fluids in a space environment. This is also applicable to other advanced radiator concepts.

In short, the space experiment is a key step in the development of MBR systems. Such systems show particularly good potential, resulting in stowable, lightweight radiators required for future NASA and DOD missions having substantial power requirements.

6.0 RELATIONSHIP TO OTHER AGENCIES AND CENTERS

The work on the MBR is part of a comprehensive investigation of advanced radiator systems. Various NASA centers such as Lewis, Johnson Space Center (JSC), and Goddard Space Flight Center (GSFC), are managing the research in these new technologies. NASA, in cooperation with the DOD, is coordinating the direction of research which is best suited for possible future missions. The main DOD centers which are interested in advanced radiator systems include the Air Force Astronautics Lab (AFAL) and Air Force Wright Aeronautical Labs (AFWAL) at Wright Patterson AFB. Currently the NASA effort is divided as follows:

- Lewis is involved with advanced heat pipes, LDR, and the MBR technologies;
- JSC is involved with advanced heat pipes, advanced heat exchangers (evaporators, condensers), two phase pumped loops, and the Rotating Bubble Membrane Radiator (RBMR) concept;

- Goddard primarily is involved with advanced heat exchangers and two phase pumped loops.

With NASA investigating the possible options for future space radiator concepts such as the MBR, LDR, and the RBMR, many similar technical obstacles exist and advancement with any one concept could also benefit the others. The MBR space flight experiment relates directly to other programs within NASA, DOD, industry, and academia directed toward the development of advanced radiator technologies. These inter-relationships include:

- The participation of multiple NASA centers and the OAST Office in establishing the interface and safety criteria which will guide the design of the experiment.
- Inclusion of the experience of DOD programs directed toward MBR applications as exemplified by the several MBR development efforts sponsored by AFAL.
- Dissemination of experimental results to companies assessing the potential for advanced radiators to enable future civilian and military missions.
- The development of a data base allowing for improvement of the analytical methods for predicting the dynamic response of "floppy" structures operating in a space environment. Such a capability is central to the evaluation and design of large space structures in general and specifically for several of the advanced radiator concepts under consideration.

Due to the interest of the space community in this and related technology, the program participants will endeavor to ensure that the experimental design is consistent with hardware that will address most of the key issues associated with dynamic characteristics of this technology.

7.0 TECHNICAL DESCRIPTION

7.1 SYSTEM DESCRIPTION

A preliminary design of the basic experimental apparatus is shown in Figures 4, 5, and 6. The components which have been identified to date are:

- An IHX with the working fluid and the required seals;
- A reservoir which will contain the working fluid during transport to low earth orbit;
- A belt made of a polymeric material which will be drawn through the IHX; the belt will be between 2.4 and 3.7 meters (8 and 12 feet) in diameter, depending on spacecraft integration requirements;
- A motor-roller arrangement which will drive the belt;
- A load cell system which will measure the forces produced by the belt and the IHX on the simulated spacecraft;
- A linear actuator which can perturb the belt so as to simulate a docking maneuver or other short term acceleration;
- A camera system which will allow photographic documentation of belt motion during deployment, normal operation, and when subjected to linear perturbations;

- A deployment mechanism which will form the belt into a roughly cylindrical shape before engaging the belt drive system;
- A retraction system which will stow the belt after testing is completed.

The list of the components must be expanded and specific items identified. Most of the components will be selected due to their survivability, reliability, and the space constraints dictated by the shuttle mission. Following are some of the considerations for the primary components.

- Belt Material: The belt must be chosen such that the dynamic response will be similar to that of a full size system. The material having the best thermal characteristics and compatibility with the space environment will be sought. Some possible belt materials include nylon, polyimides, Teflon, polypropylene, polyethylene, mylar, tantalum, and aluminum.
- Seals for the IHX: The seals that will be used should be similar to those used in previous bench-top testing (see Reference 3). The seals should be compatible with the space environment and the working fluid. Some possible seal materials include: rulon, Teflon, or some type of elastomeric compound.
- Working Fluid: A low vapor pressure fluid with relatively high thermal conductivity is essential. If the fluid is nonwetting and has high surface tension, then the seal design is simplified. Gallium meets the requirements and is, therefore, a prime candidate. Other liquids, such as mercury, will be examined for applicability to this experiment.
- Drive System: The drive motor and rollers must all be chosen based on weight, compatibility to the space environment, and performance in a MBR system. Reliability of the components must be extremely high to ensure proper operation over extended periods of operation and multiple starts and stops.
- Deployment and Retraction Mechanism: The criteria for this system are similar to that of the drive system.
- Linear Perturbation System: This will be comprised of multiple linear actuators which will have the power to accelerate the MBR to the required levels. Also, the distance that the linear actuator can displace the MBR must be sufficient to accurately model the predicted displacements that would occur in a final design, on the order of 5 to 15 cm (2 to 6 inches). The reliability must again be very high. Also, consideration will be given to the influence that the linear actuators have on the dynamic behavior of the overall MBR system.
- Measurement Equipment: Redundancy will be employed but a high reliability will still be expected of this equipment. Compatibility with the space environment and the capacity to measure the expected loads will be prime considerations. All of the equipment should be able to handle some overload due to unexpected influences, including those from shuttle launch. The effects that any measurement device has on the MBR operation should be minimized or eliminated.

All of the equipment that is selected must be able to withstand the accelerations due to shuttle take off. These are not trivial and must be accounted for both in the equipment and in the structural integrity of the experiment. In addition to these considerations, safety and weight will influence all component selections.

Operating temperatures for the linear actuators and drive system will be an important factor in deciding whether or not a heating/cooling system is required in order to maintain proper operating temperature during this experiment.

7.2 EXPERIMENT SEQUENCE

The sequence that will lead to a successful experiment is as follows:

- Deployment of Belt: When the MBR experiment is ready for operation the deployment system will be actuated, allowing the belt to form a cylindrical shape due to the centrifugal forces. The deployment of the belt will require that the motor to the storage drive rollers be disconnected via a clutch; the main drive motor will then pull the belt out of the storage box and through the IHX, feeding it out to space. This would allow the belt to deploy into a cylindrical shape.
- Operation of the MBR: The belt will be operated in its normal deployed shape for an extended period of time, the duration depending on overall mission requirements. During this period the belt speed and IHX seal forces will be varied over a predetermined range to verify the effects of these operating parameters on belt dynamics.
- Linear Perturbations: Once steady state dynamic characteristics have been measured, the actuator will move through a preestablished sequence to verify belt dynamic response when subjected to linear accelerations. A range of both displacements and acceleration levels will be explored in order to test the capabilities of the analytical models to accurately assess the impact of imposed motion. The photographic record of the belt dynamics will be particularly important during this experimental sequence.
- Thermal Testing: Thermal characteristics of the MBR would then be measured. The IHX would be filled with the working fluid and the belt would be operated under a steady state condition for a variety of gallium bath temperatures, belt speeds, etc.
- The final steps would include retracting the belt and securing the experiment for the return to earth. The retraction of the belt would require (refer to Figure 5) that the main drive motor be switched off and that the solenoid clamping system at the exit of the storage box be activated, thereby sealing the storage box. The motor connected to the storage drive rollers would then be activated and engaged via the clutch and the belt would be fed into the storage box. No internal mechanism for storing the belt in an orderly fashion is planned for the shuttle experiment; therefore, the belt would stow away in a random fashion.

7.3 REQUIRED MEASUREMENTS

The measurements that are required will fall into two categories: 1. Control and maintenance; 2. Data collection. In the area of control and maintenance the quantities to be measured will include, but not be limited to:

- Belt velocity;
- Deployment mechanism position;
- Torque output of belt drive system;
- Gallium bath temperature;
- Power input into the gallium bath, i.e. current into the electrical resistance heating, IHX wall temperature (solar load), etc.

As data collection measurements, a variety of forces and accelerations must be monitored, as well as some thermal characteristics. These will include:

- Belt temperature at entrance and exit of IHX;
- Belt motion and shape;
- IHX impulse acceleration levels;
- Reaction forces on the simulated spacecraft;
- Belt drag forces due to IHX.

An instrument tape recorder may be required due to the large volume of data, especially during thermal testing. If possible, the shuttle recording capabilities will be utilized.

7.4 DATA COLLECTION AND REDUCTION

The data collected from the experimental apparatus of Figure 5 will be:

- Verification of belt shape in the reduced gravity environment when subjected to linear motion. (Photographic documentation)
- Drag forces on the IHX and associated parasitic power due to seal pressure and variable forces during normal operation. (Load cell)
- Force fields on the IHX due to short-term linear accelerations. (Load cell)
- Damping coefficients of belt perturbations resulting from impulse linear acceleration. (Photographic documentation and accelerometers)
- Thermal characteristics of the MBR. (Thermistors)

This information will be compared to: analytical predictions (Reference 3) from a lumped parameter model which simulates belt dynamics; the projections of seal forces (parasitic power losses) as estimated by basic mechanical analyses of the functioning IHX; the thermal analysis; and ground based thermal testing.

8.0 PAYLOAD INTEGRATION

8.1 TECHNICAL REQUIREMENTS

The proposed experiment is to be conducted in the shuttle bay. This would allow for the use of a pallet, hitchhiker carrier, or spacelab module as the experiment carrier. Figure 7 shows a possible mounting configuration within the shuttle using the Hitchhiker-M platform.

The deployment of the experiment within the shuttle bay area will allow a larger belt to be tested. Figure 8 shows the deployed unit in the shuttle bay. The radiator surface should view space with minimal incident solar energy. In order to have the maximum view of space, the entire radiator surface should be above the shuttle bay doors. The view factor for the belt will have to be calculated once the elevation above the shuttle opening is known.

It is expected that at least two hours will be required to conduct a comprehensive test. The test should include as a minimum:

- Extended periods in steady state operation at various conditions (operating time of approximately 30 minutes);
- Periods of perturbation and return to steady state (operating time of approximately 1 hour);
- Thermal testing at various power levels (operating time of approximately 1 hour).

In addition to these phases of testing, a deployment and retraction sequence will have to be performed. These two steps should not require more than ten minutes total. Finalization of the test plan and required time must be negotiated with NASA personnel.

The expected mass of the experiment is detailed in Table 1. Two estimates are listed in Table 1, one for a system which will test a 3 m (10 ft.) diameter belt, and a second for a 3.7 m (12 ft.) diameter belt.

8.2 REQUIRED POWER

Table 2 lists the expected power requirements. The majority of the power will be used to drive the belt. This parasitic power in the system is due to the drag forces within the IHX, and to a lesser extent, the drag forces of the rollers. The highest level of power during the dynamic testing will be associated with the deployment of the belt. It is at this time that all drag forces will be present as well as the requirement to accelerate the belt to speed.

A specific temperature (approximately 320 K) will be required within the bath so that evaluation of the thermal characteristics can be achieved. One option for heat input would be to use an electrical resistance heating element in the bath with a control system. Another possible option is the use of solar heating as the power input for the gallium bath, thereby reducing the requirement for onboard power. The power required for electrical resistance heating is relatively high and may require additional battery packs. The most straightforward approach would be to use shuttle power with, if required, additional battery packs. The belt material will have to be chosen (proper emissivity)

TABLE 1: MASS OF PROPOSED EXPERIMENT

Item	Mass[1] kg (lbm.)	Mass[2] kg (lbm.)
Belt	2.5 (5.5)	3.6 (7.9)
Main Drive System	11.9 (26.2)	13.9 (30.6)
IHX (seals & box)	8.3 (18.3)	10.0 (22.0)
Gallium Container and Gallium	9.3 (20.5)	10.8 (23.8)
Storage/Deployment Mechanism	19.3 (42.5)	19.9 (43.8)
Total[3]	51.3 (113.0)	58.2 (128.1)

[1]Mass of system with 3 meter (10 foot) diameter belt and thermal testing.
[2]Mass of system with 3.7 meter (12 foot) diameter belt and thermal testing.
[3]No carrier has been included in this total.

TABLE 2: POWER REQUIREMENTS FOR THE PROPOSED EXPERIMENT

Item	Required Power[1] (watts)	Required Power[2] (watts)
Drive System	150.0	150.0
Maintenance Data	100.0	100.0
Test Data	100.0	100.0
IHX Heater[3]	1000.0	1400.0
Total	1350.0	1750.0

[1]Power requirement of system with 3 meter (10 foot) diameter belt and thermal testing.
[2]Power requirement of system with 3.7 meter (12 foot) diameter belt and thermal testing.
[3]Not required if thermal testing is eliminated.

such that excessive power is not required for thermal testing. For the power requirement estimate of Table 2, an emissivity of 0.5 and an average belt temperature of 320 K was assumed. A first estimate of the view factor from the entire belt surface area to space was 0.45. Once the actual configuration and belt size are selected, a more detailed analysis can be completed. A heater may be required for the working fluid container to ensure that the fluid remains melted while being transferred to the IHX. This will depend on the final selection of a working fluid and on the shuttle orientation before and during the fluid transfer.

The remainder of the required power will be for data collection. Due to the need for force, drag, velocity, and thermal measurements, some power will be required as excitation voltages and as power for recording media.

8.3 REQUIRED SUPERVISION

The experiment is expected to require minimal direct supervision. Transfer of the working fluid from the storage container to the IHX will be required. All measurements and deployment sequences can be automatic once out of storage and activated, but some basic manual switching may be required. Monitoring by mission specialists will be required to ensure that the experiment progresses as planned. No extravehicular activity is expected since all switching can be completed from the aft flight deck.

8.4 ORBIT REQUIREMENTS

In order to perform the dynamic testing it will be necessary to keep the angular rotations and accelerations to a minimum during operation. The temperature requirements of the MBR during the dynamic testing may require that the shuttle rotate during its orbit in order to maintain a moderate temperature environment.

During the thermal testing the radiator surface should have minimal incident solar energy. This would require that the shuttle bay be facing away from the earth and the sun.

9.0 SUPPORTING DATA/REFERENCES

The experimental design has been initiated with preliminary results indicated in Section 7.0. The background analyses leading to the development of MBR designs and understanding of deployment and operational issues are contained in the following reports prepared by ADL for NASA Lewis:

1. "Preliminary Evaluation of a Liquid Belt Radiator for Space Applications," NASA CR-174807, December, 1984.
2. Teagan, W.P. and Fitzgerald, K., "Liquid Belt Radiator Design Study," NASA CR-174901, January, 1986.
3. "Moving Belt Radiator Technical Development, Final Report," to be published as NASA CR-xxx, for NASA Contract NAS3-24650, 1990.
4. Aguilar, J.L., "Conceptual Design of MBR Shuttle-Attached Experiment, Final Report," NASA CR-185169, 1989.

APPENDIX A

DYNAMIC ANALYSIS OF MOVING BELT RADIATOR

This appendix discusses the analysis and computer model developed at Arthur D. Little to model the dynamics of the belt.

A.1 STEADY-STATE MOTION

As shown in Figure 9, the steady-state shape of the belt will be cylindrical[1] and all elements in force equilibrium. Thus, for a segment dx, a force balance in the radial direction yields:

$$F = T_1 \sin\frac{\theta}{2} + T_2 \sin\frac{\theta}{2}$$

where F is the centrifugal force on the element defined as:

$F = \rho A dx \quad V^2/R$ $\qquad$ A = *Belt Cross Sectional Area*

R = *Belt Radius* $\qquad$ ρ = *Density*

V = *Tangential Velocity*

If no tangential acceleration is assumed, a force balance in the tangential direction yields:

$$T_1 \cos\frac{\theta}{2} = T_2 \cos\frac{\theta}{2}$$

or $T_1 = T_2 = T$

substituting $\theta = \frac{dx}{R}$

and assuming $\sin\theta \cong \theta$

we finally obtain: $T = \rho A V^2$

---

1 This does not take into account (i) any tension force caused by an imbalance between the centrifugal force and gravitational force (important for a large belt circulating in the radial direction), (ii) variations in belt properties due to liquid phase change and (iii) the effects of Coriolis acceleration. These are discussed below.

indicating the tension in the belt is proportional to mass per unit length velocity squared.

A.2 DYNAMIC RESPONSE ISSUES

As mentioned earlier, the objective of the dynamic analysis is to study the response of the belt to external effects and spacecraft generated forces. These forces can generate in-plane or out-of-plane motion of the belt as discussed next.

A.2.1 External Effects

Two of the external effects to be considered are:

- The acceleration generated by gravity/centrifugal force imbalance.
- The Coriolis acceleration effects.

A.2.1.1 The Force Imbalance

The acceleration generated by gravity, centrifugal force imbalance is explained in Figure 10. As shown in the figure, we have assumed that the center of gravity (cg) of the spacecraft/belt system lies in the spacecraft. Now, if we assume that the spacecraft is in a circular orbit at distance r_{cg} from the center of earth, then the force balance dictates:

$$\text{centrifugal force} = \text{gravitational force}$$

$$M\omega^2 r_{cg} = MM_e G/r_{cg}^2 \qquad \text{(A.1)}$$

where M = mass of the system

M_e = mass of the earth

G = gravitational constant

ω = angular velocity of spacecraft

$$\text{From Equation (A.1), } \omega^2 = M_e G/r_{cg}^3 \qquad \text{(A.2)}$$

Now, Point A on belt will also rotate around earth at the same angular velocity ω, however, since Point A is at radius r_a, which may not be the same as radius r_{cg} of the center of gravity, the gravitational force will not cancel the centrifugal force[2]. For $r_a > r_{cg}$, the centrifugal force will be higher than the gravitational force. (The reverse will be true for $r_a < r_{cg}$.) The acceleration due to this imbalance, a_i will be

$$a_i = \omega^2 r_a - M_e G / r_a^2 \qquad \text{(A.3)}$$

Substituting the value of ω from Equation (A.2) and rearranging

$$a_i = \frac{M_e G}{r_a^2} \left[\left(\frac{r_a}{r_{cg}} \right)^3 - 1 \right] \qquad \text{(A.4)}$$

For typical values of r_a, r_{cg}, M_e and G, the value of a_i is indeed quite small -- of the order of 2×10^{-5} m/sec^2. Thus, this effect must be considered only for very large belts.

A.2.1.2 The Coriolis Acceleration

Coriolis acceleration will exist any time a point within a rotating frame of reference has a relative velocity with respect to the frame of reference. This acceleration is given by:

Coriolis acceleration = $a_c = 2\omega \times V_{rel}$

where ω is the angular velocity of the frame with respect to the inertial frame and V_{rel} is the relative velocity.

Now, every point in the belt has a relative velocity with respect to the spacecraft which is rotating around earth. Assuming spacecraft rotation once every hour and V_{rel} equal to 1 m/sec, the magnitude of the Coriolis acceleration is 0.00174 m/sec^2. For a belt with radius 6.49m, the centripetal acceleration on belt is 0.154 m/sec^2, which is 88 times the Coriolis acceleration. Thus, the effects of the Coriolis acceleration can be neglected in the initial analysis.

A.2.2 Spacecraft Motion

The spacecraft can translate or rotate along any of the three axes shown in Figure 9. Also, it can execute a motion which includes any combination of these. For this initial investigation, we restrict ourselves to the uncoupled motions.

2 The centrifugal force due to belt rotation is cancelled out by the belt tension force and not included in this analysis.

Also, at this point, it is important to make distinction between vibrations and gross deformations. A relatively small motion of the spacecraft can set up vibrations in the belt. For example, a motion in Y direction can start bending vibrations in the belt, as shown in Figure 11(a). A study of these vibrations; their modes, frequencies and damping constants; is useful while preparing a final design of the belt. At this stage, however, it may be more important to study the gross deformation of belt due to large displacements of spacecraft such as that shown in Figures 11(b) and (c).

Such deformations can cause a permanent crease in the belt or harm its structural integrity. If this happens while the spacecraft is executing a realistic motion, the integrity of the whole radiator will be in jeopardy. The same cannot be said about the vibrations in the belt. They may lead to certain temporary performance deterioration, but generally not to a system failure. Thus, we have put emphasis on studying the gross motion in this task.

We next make qualitative observations about gross deformation in belt due to spacecraft motions along the three axes and rotation along each axes.

A.2.2.1 In-Plane Motion

The translation of spacecraft along the X, Y axes and rotation around the Z axis will produce in-plane motion of belt. This motion is somewhat less complex to analyze than the out-of-plane motion produced by the other three types of spacecraft motion. As discussed above, translation along the Y axis will produce motion such as that shown in Figure 11. A large acceleration along the X axis will probably produce a belt shape as shown in Figure 12(a) leading to a crease type failure near entry or exit from the spacecraft. Rotation around the Z axis will still produce in-plane motion of the belt, but now the danger may be a crease type failure at spacecraft entry or exit, or belt wrapping on itself (see Figure 12(b)).

A computer program has been developed to understand the in-plane motion of the belt which will be described later. Thus, the discussion of this type of belt behavior is deferred until then.

A.2.2.2 Out-of-Plane Motion

As discussed earlier, we have not analyzed the out-of-plane motion in any great depth. However, some observations about this can be made. The motion of the spacecraft along the Z axis will produce a somewhat complicated response in the belt. The belt will resist motion because of inertia and that will in effect produce a shear force and torque along the X axis near spacecraft entry and exit points. This will cause a twist in the belt and, potentially, a damaging crease, as shown in Figure 13(a).

That torque on the belt near the spacecraft can be expressed as:

$$\text{Torque} = M_b Z R_b$$

Where M_b = Belt mass
R_b = Belt radius
Z = Belt cg acceleration along the Z axis

Now, if τ_c = torque needed to cause permanent damage, the critical value of acceleration will be:

$$Z_{critical} = \tau_c / (M_b R_b) \quad = \tau_c / (M_b R_b) \qquad (A.5)$$

As long as the spacecraft motion keeps the belt cg acceleration under this value, the belt will not be damaged. Laboratory data on belt compliance in twist and torque required to cause permanent damage are needed to obtain acceleration threshold along the Z axis.

However, to get a very rough estimate on critical Z axis acceleration, we made the following assumptions:

- The belt fails in twist because the peak shear stress in the belt at belt edges exceeds the shear yield limit, assumed to be 1×10^8 N/m^2 (15,000 psi).
- Shear stress at any location in the belt is proportional to its distance from belt mid-line.

Then, the following equation holds well:

$$\tau_c = \text{shear yield limit} \times 0.5W^2 \times t \times 0.667 \qquad (A.6)$$

Where W = belt width
t = belt thickness

For a belt composed of fabric with 0.02" (0.05mm) dia. strands, 10 strands per inch, t equals 8×10^{-5}m. Assuming belt width to be 3.3m, belt mass to be 82 kg and radius to be 6.5m,

$$\tau_c = 1.4 \times 10^4 \text{ N-m}$$

$$\text{and } Z_{critical} = 27.2 \text{ m/sec}^2 = 2.8 \text{ g}$$

Remember, this is a very rough estimate based on an assumption that the "weakest link in the chain" in Z axis acceleration is shear failure at belt outer edge near spacecraft entry or exit which may not be true; the belt may get tangled at a much lower acceleration level. However, this analysis indicates that the belt can take substantial acceleration levels along the Z direction. This is important to note when the in-plane acceleration levels are examined.

The rotational acceleration along the X axis will produce an effect on the belt similar to that produced by the translational acceleration along the Z axis (see Figure 13(b)). Torque created by such motion on the belt at spacecraft entry-exit points will be:

$$\text{Torque} = \alpha I_{AA} \qquad \text{(A.7)}$$

I_{AA} = Belt moment of inertia along an axis passing through the spacecraft and parallel to the X axis.

If the critical torque level is assumed to be 1.4×10^4, and I_{AA} to be 5200 kg-m^2, peak angular acceleration along the X direction is:

$$\alpha = 14000/5200 = 2.7 \text{ rad/sec}^2$$

This is a very high acceleration level and we believe that the belt will fail because of some other mode (e.g., getting tangled) prior to failure due to shear stress when the spacecraft is rotated along the X axis.

Finally, the rotation of the spacecraft along the Y axis produces a complex response in the belt, particularly if the rotational acceleration is significant. The failure mode in this case could be buckling on the belt sides. Some laboratory tests are needed to determine buckling limits of the belt and hence the critical acceleration levels. Our engineering judgment is, however, that the belt will be able to take relatively large rotational acceleration levels along the Y axis.

A.3 DYNAMIC MODEL OF IN-PLANE MOTION

While selecting the best way of modeling the in-plane motion of the belt, we considered various options.

We decided very early in the project not to attempt to develop a distributed closed-form model of the belt. Lallman of Langley Research Center has performed a detailed analysis of vibration characteristics of a steadily rotating slender ring[3]. As it is, this analysis is very complex. The MBR incorporates additional complications of (i) constraints to the motion due to travel inside the spacecraft and (ii) nonlinear characteristics of a two-phase belt. These would make any search for a closed form solution prohibitively complicated, and very likely, futile.

Thus, we decided, instead, to use a lumped parameter approximation. Figure 14 shows the lumped parameter representation of the MBR belt for investigating the in-plane motion. As can be seen, the belt is divided into lumped masses connected by:

---

3 Lallman, F.J., "Vibration Characteristics of a Steadily rotating Slender Ring", NASA Technical Paper 1775, NASA, December 1980.

- Linear springs and dampers representing belt elasticity and damping in the tension/compression mode.

- Rotational springs and dampers representing belt stiffness and damping in the bending mode.

The dynamic equations of motion of the belt then are nothing but a collection of equations of motion for each lumped mass in X and Y direction, i.e.:

$$\ddot{Y}_i = \Sigma F_{yi}/M_i \qquad \text{(A.8)}$$

$$\ddot{X}_i = \Sigma F_{xi}/M_i \qquad \text{(A.9)}$$

Where ΣF_{yi} and ΣF_{xi} are, respectively, summations of the Y and X direction components of forces acting on the *i*th mass.

M_i = mass of the *i*th mass

Note that all displacements, velocities and accelerations are referred to the inertial frame.

The forces on the masses can arise from the bending or linear springs and dampers (shown in Figure 14) or from the spacecraft.[4] The spacecraft provides forces necessary to impart a velocity to the belt so that it can perform its function as a radiator. Additional forces are imparted when the spacecraft moves (beyond its steady rotation around earth). The spacecraft imparted forces, however, depend on the detailed designs of bath and drive mechanism which are not yet finalized. In the model developed, we bypassed the problem of having to specify the forces that would act on the belt inside the spacecraft by assuming that the spacecraft imposes displacement and velocity constraints on the part of the belt inside the spacecraft, with forces assumed to be such that these constraints are observed.

$\ddot{Y}_i$ Y direction of the *i*th mass

$\ddot{X}_i$ X direction of the *i*th mass

The forces acting on the lumped masses are as shown in Figure 15. In the figure:

$F_{ki} = K_i (d_i - l_i)$ for $d_i > l_i$

4 The centrifugal "force" is incorporated automatically when belt is imparted a velocity of rotation.

$= 0$ for $d_i \leq l_i$ (A.10)

where l_i = initial length of link i,

k_i = linear stiffness (elasticity) of link i,

F_{ki} = linear stiffness force in link i,

and d_i = stretched length of link i.

$$d_i = ((X_{i+1} - X_i)^2 + (Y_{i+1} - Y_i)^2)^{\frac{1}{2}} \quad \text{(A.11)}$$

where X_i, Y_i = coordinates of mass i

$$K_i = E_t A/l_i \quad \text{(A.12)}$$

where E_t = belt modulus of elasticity in tension

A = area of cross section of belt

Similarly, the damping force in link i, F_{Di}, is given by

$$F_{Di} = V_i B/l; \quad \text{(A.13)}$$

where B = damping coefficient of a one meter long belt in stretching

V_i = stretching velocity of link i

$$V_i = (V_{xi+1} - V_{xi}) \cos \theta_i + (V_{yi+1} - V_{yi}) \sin \theta_i \quad \text{(A.14)}$$

where V_{xi}, V_{yi} = X and Y direction velocities of mass i

$$B = 2 \pi \xi \sqrt{AE_t \mu} \quad \text{(A.15)}$$

where ξ = damping ratio of first natural frequency in stretching

μ = linear mass density of belt (kg/m).

Similarly, the forces acting on the lumped masses due to belt bending are given by:

$$F_{1i} = (K_{li}\psi_i + B_{li}\dot{\psi}_i)/d_{i-1} \quad \text{(A.16)}$$

$$F_{2i} = (K_{li}\psi_i + B_{li}\dot{\psi}_i)/d_i \quad \text{(A.17)}$$

where

K_{li} = belt bending stiffness at mass i

B_{li} = belt bending damping coefficient at mass i

$\psi_i = \theta_i - \theta_{i-1}$ = bending angle (A.18)

$\dot{\psi}_i$ = rate of bending angle change

$K_{li} = E_b I / l_i$ (A.19)

$B_{li} = B_l / l_i$ (A.20)

where E_b = modulus of elasticity in bending

I = belt section modulus

B_l = damping coefficient for one meter long belt in bending

Also, for a belt made out of a mesh material,

$$B_l = 4 B r_f / 3\pi \quad (A.21)$$

where r_f = strand radius

The forces given by Equations (A.10), (A.13), (A.16) and (A.17) are decomposed into X and Y components and added together so that mass accelerations in the X and Y directions can be obtained using Equations (A.8) and (A.9).

The constraints imposed by the spacecraft, for every mass inside the spacecraft, are given by (see Figure 16):

$$\ddot{X}_i = \ddot{X}_s - 2V\sin(\Omega)\dot{\Omega} - \ddot{\Omega}X_{bi}\sin(\Omega) - \dot{\Omega}^2 X_{bi}\sin(\Omega) \quad (A.22)$$

$$\dot{X}_i = \dot{X}_s + V\cos(\Omega) - X_{bi}\sin(\Omega)\dot{\Omega} \quad (A.23)$$

$$X_i = X_s + X_{bi}\cos(\Omega) \quad (A.24)$$

$$\ddot{Y}_i = \ddot{Y}_s + 2V\cos(\Omega)\dot{\Omega} + \ddot{\Omega}X_{bi}\cos(\Omega) - \dot{\Omega}^2 X_{bi}\sin(\Omega) \quad (A.25)$$

$$\dot{Y}_i = \dot{Y}_s + X_{bi}\cos(\Omega)\dot{\Omega} + V\sin(\Omega) \quad (A.26)$$

$$Y_i = Y_s - H + X_{bi}\sin(\Omega) \quad (A.27)$$

where

X_i, $\dot{X}_i$, $\ddot{X}_i$ = displacement, velocity and acceleration along inertial X axis for mass i

Y_i, $\dot{Y}_i$, $\ddot{Y}_i$ = the above along inertial Y axis

Ω, $\dot{\Omega}$, $\ddot{\Omega}$ = spacecraft angular displacement, velocity and acceleration around inertial Z axis

X_s, $\dot{X}_s$, $\ddot{X}_s$ = spacecraft displacement, velocity and acceleration along inertial X axis

Y_s, $\dot{Y}_s$, $\ddot{Y}_s$ = the above along inertial Y axis

X_{bi} = distance of lumped mass i from spacecraft center

H = height of belt center above liquid bath inside spacecraft

V = belt velocity.

This model was coded and converted into a computer simulation which generates snapshots of the belt starting from an initial condition to any desired time subsequent to application of spacecraft motion.

At this point it should be noted that the belt designs under consideration incorporate materials which are quite inelastic. This causes a problem in performing computer simulations: the time required for calculations is quite small, thus a significant amount of computer time is needed to perform simulations. We tried to address this problem by developing a model which assumes the belt to be made up of inelastic, rigid links connected with each other by hinges bending stiffness and damping. This model, however, is quite complex and requires detailed information on forces acting on the belt while inside the spacecraft. Such forces cannot be provided while the designs of bath and drive mechanism are under development. Therefore, we had to abandon, at least temporarily, this other model and continue using the model discussed above which, while slow and time consuming, is appropriate for this stage of belt development.

A.4 COMPUTER PROGRAM SUMMARY

A computer program, titled Belt Radiator Simulation Program (BERS), was developed to simulate the in-plane dynamic performance of the belt radiator. This program incorporated the lumped-parameter model, described in the preceding subsection, and used a Runge-Kutta fourth order integration algorithm to generate plots of belt shape for a variety of belt parameters and spacecraft motions.

The input parameters for the program include:

- Number of lumped masses (N),
- Belt width (W),
- Belt drive length (2 max X_{Bi}),
- Belt length (unstretched) (Nl_i),
- Belt material density (mass per area) (μ/W),
- Modulus of elasticity of belt material in tension (E_t),
- Modulus of elasticity of belt material in bending (E_b),
- Belt area of cross section (A),
- Belt section modulus ($\bar{I}$),
- Damping ratio for first stretching vibration mode (ξ),
- Radius of strand (for mesh type belt) (r_f),
- Velocity of rotation (V), and
- Spacecraft motion parameters (acceleration magnitude, direction, duration)

The output of the program can include, if desired, a printout of displacements, velocities and acceleration of any lumped mass, plus the forces acting on any mass. However, the preferred output includes plots, similar to that shown in Figure 2, of belt shape at any time.

APPENDIX B

POINT DESIGN EQUATION DEVELOPMENT AND ANALYSIS METHODOLOGY

The development of the point design Equations is presented in this appendix. Although applied to the particular mission defined in Reference 1, the formulations given here are sufficiently general to be of use in any Moving Belt Radiator design.

B.1 RADIATIVE HEAT TRANSFER EQUATIONS

For this analysis, the initial assumptions which are made are: 1) the radiator is shaped like a cylindrical hoop; 2) the radiator surfaces are edge on to the sun; and 3) no net exchange between radiator elements that view each other are made. The radiative exchange between a radiative element having a projected area dA_s and its equivalent black-body surroundings is given by the relation:

$$dQ_{net} \equiv 2\,\sigma F_{RS}\,\varepsilon_R\left[T_R^4 - \frac{\alpha_{RS}}{\varepsilon_r}T_s^4\right]dA_s \qquad \text{(B.1)}$$

where:

- ε_R is the total hemispherical emissivity of the radiator surfaces;
- α_{RS} is the absorptivity of the radiator surface to the radiation from its surroundings;
- F_{RS} is the combined view factor of the radiator surface element $2dA_R$ to its surroundings (same for all elements);
- T_R is the temperature of the radiator element;
- T_S is the equivalent black-body temperature of the surroundings;
- σ is the Stefan-Boltzmann constant.

Making the further assumption that the spectral character and the radiant flux emitted by the surroundings is that of a black-body having a temperature near that of the radiator and evoking Kirchoff's Law, $\alpha_{RS} / \varepsilon_R$ is approximately unity. Therefore Equation (B.1) reduces to:

$$dQ_{net} \equiv 2\,\sigma F_{RS}\,\varepsilon_R\,[T_R^4 - T_s^4]\,dA_s \qquad \text{(B.2)}$$

The radiation actually coming from the surroundings may include that in the visible range (reflected sunlight from the earth and spacecraft) as well as that in the infrared range (emitted from the earth and spacecraft). A refined analysis would consider the spectral character of the radiation from the surroundings incident on the radiator and its absorptivity to it. For example, assume that the surroundings have an incident flux equal to that of a black-body at 250K but has 30 percent of the energy due to reflected sunlight (Earth's albedo) and the remainder resulting from radiation from nearby bodies at 300K. In this example a radiator using vacuum oil would have an absorptivity to the long wavelength radiation near unity and an absorptivity/emissivity ratio in the visible band near 0.1, resulting in an effective $\alpha_{RS} / \varepsilon_R = 0.73$ and an effective black-body temperature of 231K.

This lower effective temperature of the surroundings reduces the radiator area required to reject a specified amount of heat by 8 percent from that calculated on the basis of Equation (B.1) with T_S = 250K. Similarly, a Liquid Belt Radiator using gallium operating in the sensible heat mode has an estimated absorptivity/emissivity ratio in the visible band of 3, an effective $\alpha_{RS} / \varepsilon_R = 1.6$, and an effective black-body temperature of 281K. In this case, Equation (B.2) underestimates the required radiator area by 11 percent.

B.2 MBR GEOMETRICAL RELATIONSHIPS

To further simplify, Equation (B.2) was linearized about the maximum operating temperature. This linearization was assumed valid for the temperature ranges and variations considered in this analysis. The quartic temperature difference ($T_R^4 - T_S^4$) may be expressed as:

$$T_R^4 - T_S^4 = (T_R^2 + T_S^2)\,(T_R - T_S)\,(T_R + T_S)$$

or in the final form:

$$T_R^4 - T_S^4 = T_R^3\,(b)\,(T_R - T_S)$$

In this case:

$$b = 1 + \left(\frac{T_s}{T_R}\right) + \left(\frac{T_s}{T_R}\right)^2 + \left(\frac{T_s}{T_R}\right)^3$$

where T_R^3 is the linearized constant term fixed at the maximum belt radiating temperature occurring at the exit of the bath heat exchanger. Thus, the net differential radiative exchange equation may be rewritten in linear form as:

$$dQ_{net} = 2\,\sigma F_{RS}\,\varepsilon_R\,b\,(T_{RMAX})^3\,(T_R - T_S)\,dA_s \qquad \text{(B.3)}$$

Where T_R is the radiating temperature of the differential area dA_S

Figure 17 portrays this differential area. This segment may be used to determine the energy transfer for the entire MBR system. Using a differential form of the first law, we may write:

$$\dot{m}\,c_p\,dT_R = -Q_R''\,(w \cdot dx) \qquad \text{(B.4)}$$

where:

- w is the width of the radiator belt (Figure 17);
- dx is the differential length in the direction of belt travel;
- dT_R is the temperature variation across the differential control volume;
- $\dot{m}$ is the mass flow of the belt material;
- Q_R'' dQ_{NET}/dA_S, or the net energy flux rate from the differential element.

Since the material flow rate can be written as:

$$\dot{m} = \rho\,V\,t\,w$$

where:

ρ is the density of the working fluid;

V is the tangential belt speed;

t is the belt thickness;

w is the belt width.

Equation (B.3) can be reformulated to:

$$\frac{dT_R}{dx} = \frac{2F_{RS}\,\sigma\,\varepsilon_R\,b\,(T_{RMAX})^3\,(T_R - T_S)}{t\,\rho\,V\,c_p} \tag{B.5}$$

The variation of the radiator temperature over the length of the belt expressed in the above equation may now be easily solved by the separation of variables technique. (Assuming the properties ε, c_p, ρ, t and F_{RS} do not vary with position x.) If the initial condition is given as:

$$T_R(x=0) = T_{RMAX}$$

The solution of the differential equation, expressing belt temperature as a function of position, may be written as:

$$T_R(x) - T_S = [T_{RMAX} - T_S]\; e^{-\psi x} \tag{B.6}$$

where:

$$\psi = \frac{2F_{RS}\,\sigma\,\varepsilon_R\,b\,(T_{RMAX})^3}{\rho\,V\,c_p\,t}$$

ψ however may be written in such a way as to greatly simplify Equation (B.5). Since an overall first law balance on the radiator implies:

$$Q_R = \rho\,V\,c_p\,t\,\Delta T_{RAD}$$

then

$$\rho\,V\,c_p\,t = \frac{Q_R}{w\,(\Delta T_{RAD})}$$

where:

ΔT_{RAD} is the temperature difference over the entire length of the belt.

Q_R is the total net radiative heat transfer.

This allows ψ to be re-expressed as:

$$\psi = \frac{2F_{RS}\,\sigma\,\varepsilon_R\,b\;w\,(T_{RMAX})^3\,(\Delta T_{RAD})}{Q_R}$$

or

$$\psi = k\,w$$

This causes Equation (B.6) to become:

$$T_R(x) - T_S = [T_{RMAX} - T_S]\; e^{-kwx}$$

or over the entire length of the belt:

$$T_R(l) - T_S = [T_{RMAX} - T_S]\; e^{-kwl} \tag{B.7}$$

Since, $w \cdot l \;=\; A_s$

where A_s is the single sided radiator area, Equation (B.6) may be used to generate this area directly. Thus:

$$A_s = \frac{1}{k}\, ln\left(\frac{T_{RMAX} - T_s}{T_{RMIN} - T_s}\right) \tag{B.8}$$

where:

$$k = \frac{2\,F_{RS}\,\sigma\,\epsilon_R\,b\;(T_{RMAX})^3\,(T_{RMAX} - T_{RMIN})}{Q_R}$$

and:

$$T_{RMIN} = T_R\,(l)$$

It must be noted that all of the above terms are either given or derived properties based on such specific criteria as minimum evaporation mass loss, etc. This is true except for the view factor of the radiator with respect to space, F_{RS}, which must be selected. For the cylindrical hoop LBR design, the selection of a view factor defined a particular geometrical relationship between the diameter and width of the cylindrical structure. For example, a view factor of 0.9 resulted in a ratio of the diameter to width of four. From the single sided area, A_s derived in Equation (B.8), the diameter, width, and circumference of the cylindrical LBR may be determined. Specifically:

$$A_s = l \cdot w = \pi \cdot D \cdot w \tag{B.9}$$

where now D and w (the diameter and width of the LBR) are interrelated by the view factor.

The mass of the LBR follows quite readily from this formulation, since:

$$M_{LBR} = \rho \cdot A_s \cdot t \tag{B.10}$$

The density of the LBR only includes that of the working fluid, with any screen mass effects ignored. Analysis has shown this approximation to be reasonable in the case when an oil is used in conjunction with a plastic mesh structure. Different material combinations, metals and plastics for example, must be carefully examined to determine their individual effects on the mass of cylindrical ribbon structure. A similar equation can be used for a solid belt radiator, the only difference being that ρ is now the density of the belt material.

B.3 BELT SPEED DETERMINATION

The speed of the belt may be determined from the first law relation applied over the length of the belt. In this case:

$$Q_R = \rho V c_p \delta w$$

or

$$V = \frac{Q_R}{\rho t c_p w (T_{RMAX} - T_{RMIN})} \tag{B.11}$$

For the point design (Q_{RAD} = 75 kw_t), the belt speed was determined to be 0.8 m/s (2.5 fps).

B.4 INTERFACE HEAT EXCHANGER SIZING

An important component of the LBR system design was the interface heat exchanger. This heat exchanger was to provide the means for the transfer of Brayton power cycle reject heat to the LBR working fluid for eventual dissipation in space. It is predicted that both heat and mass transfer will act as energy transfer modes in this system. For purposes of analysis, however, the former phenomenon only was used as a basis for design thus resulting in more conservative exchanger size estimates.

The heat exchanger design was based on compact heat exchanger theory (Reference 2). The device was a counter flow model with the Brayton power cycle fluid being pumped through tubes in a direction opposite to the direction of belt travel. Figure 18 schematically portrays this component. From this figure it may be seen that there are two sides available for heat exchange.

Using the general form for convective heat transfer, we may write:

$$Q = U A \Delta T \tag{B.12}$$

where:

- Q is the amount of heat to be transferred;
- ΔT is a temperature difference which accounts for the temperature variation of each stream as it moves through the exchanger;
- U is the overall heat transfer coefficient;
- A is the area available for heat transfer.

In order to account for the change of temperature of a stream as it moves through the exchanger, the log mean temperature difference concept was used (Reference 3). This is defined as:

$$LMTD = \frac{\Delta T_a - \Delta T_b}{ln\,(\Delta T_a / \Delta T_b)} \tag{B.13}$$

For the point design conditions specified, Figure 19 depicts the temperature differences ΔT_a and ΔT_b occurring at the interface heat exchanger.

Evaluation with respect to these values gives:

LMTD = 52.7 K

The overall heat transfer coefficient U was assumed to be 567.6 $W/M^2 \cdot K$ (approximately 100 $Btu/hr \cdot ft^2 \cdot °F$). This value was believed readily attainable and in fact somewhat conservative for the interface heat exchanger.

Employing these results and assumptions allows a heat exchanger area to be calculated. This area however may be re-expressed as:

$$A_{HX} = 2\,w\,L_{HX}$$

where:

w is the width of the heat exchanger (assumed to be the same as the width of the belt determined in Section B.2)

L_{HX} is the length of the heat exchanger in the direction of belt travel.

The "2" in the above formulation accounts for the two sides available for energy transfer. Employing these many results leads to the relationship:

$$L_{HX} = \frac{Q}{2\,U\,w\,(LMTD)} \tag{B.14}$$

or more specifically:

$$L_{HX}(m) = \frac{Q\,[kw] \cdot 10^3}{59825\,w\,[m]}$$

For the point design, this equation was used to calculate a heat exchanger length of 0.37 m (1.21 ft) corresponding to a total area of 2.51 m^2 (27.0 ft^2).

B.5 PARASITIC POWER LOSSES

The parasitic power refers to the rate of energy required to overcome the drag forces encountered as the belt moves through the bath. This analysis assumes the existence of Couette flow with a linear velocity distribution across the gap of the interface heat exchanger. The power required to overcome viscous drag was written as:

$$P = \frac{\mu V^2}{a} 2\,w\,L_{HX} \tag{B.15}$$

where:

μ is the viscosity of the working fluid;

V is the speed of the belt;

w is the width of the belt;

L_{HX} is the length of the heat exchanger as calculated in Section B.4;

a is the single sided gap distance from the top heat exchanger plate to the surface of the belt structure.

To account for other drag forces including bath containment seals (i.e. wipers), bearing drag, etc., the viscous drag defined in Equation (B.15) was doubled. Thus the total system power required to overcome all sources of drag may be written as:

$$P = \frac{\mu V^2}{a} 4 w L_{HX} \tag{B.16}$$

For the purposes of this analysis, the viscosity μ was assumed to be a logarithmic function of temperature (Figure 20). The value used in the calculations was determined from the arithmetic mean temperature of the bath for particular inlet and outlet conditions.

For the point design, temperatures of 330K at the outlet and 300K at the inlet resulted in an average viscosity for the working fluid of 1.75 N•s/m (0.0365 lb_f•s/ft^2). Employing this result along with the other relations determined in this appendix, a gap width of 0.56 cm (0.22 inch) resulted in a total parasitic loss of less than 1 kw. The actual power required to overcome this 1 kw would be at most 33% higher depending on the efficiency of the motor(s) used to drive the belt. It should be noted that alternative interface heat exchanger designs are possible which not only provide the required heat transfer but minimize drag losses.

B.6 ORBITAL AERODYNAMIC DRAG

An estimate of the aerodynamic drag force on the LBR can be gained by considering a model consisting of a normal plane area travelling through a rarefied atmosphere at orbital velocity. Attention is focused on aerodynamic conditions at an orbital altitude of 270 nautical miles, where (Reference 4):

orbital velocity, V_o	= 7.9 km/s
mean molecular weight of atmosphere, M	= 18.3 (principally atomic and molecular oxygen and nitrogen)
average particle mass, m	= 3.04×10^{-23} g
mean free-path of particle	= 10^4 m
average particle velocity	= 1.4 km/s
particle concentration, n	= $10^8/cm^3$

As the mean free path is much greater than any radiator dimension, the radiator operates in the free-molecular flow regime. The drag force can be computed by considering the momentum exchange of particles colliding with the radiator surface. As the orbital velocity is much larger (approximately 8 times) than the particle velocity, the pressure at the radiator surface is determined by the orbital speed. Assuming that the collisions of particles with the surface are elastic and reflected diffusely, the pressure on the front face of the normal area is:

$$P = nmV_o\left(V_o + \frac{V_o}{3}\right) = \frac{4}{3} nmV_o^2 \tag{B.17}$$

and the pressure on the back surface is insignificant. Accordingly, an estimate of the drag force on the LBR is given by:

$$F_D = PA_p = \frac{4}{3} A_p nmV_o \qquad \text{(B.18)}$$

where:

F_D is the aerodynamic drag force;

A_p is the area projected normal to the orbital velocity other quantities as previously defined.

Substituting the appropriate numerical values, we get

$$\frac{F_D}{A_p} = 2.53\ x\ 10^{-5}\ N/m^2$$

It may be of interest to note that the drag in free-molecular flow (calculated from Equation (B.18)) is 2.67 times that appropriate to a bluff body (drag coefficient equal to unity) in a continuum flow having the same density and approach velocity.

B.7 REFERENCES TO APPENDIX B

1) Preliminary Evaluation of a Liquid Belt Radiator for Space Applications, NASA Contractor Report 174807, December, 1984.

2) Kays and London, Compact Heat Exchangers, Figure 2-12.

3) Rohsenow, W and H. Choi, Heat Mass and Momentum Transfer, 1961, page 310.

4) Santeler, D.J., Et Al, "Vacuum Technology and Space Simulation," NASA SP-105, 1966.

APPENDIX C

VIEW FACTOR RELATIONSHIP FOR CYLINDRICAL MBR

The MBR point design, a 75 kW radiator which is discussed in Reference 1, is based on the assumption that the radiator is in a cylindrical configuration of radius R, and axial dimension (or width), W. For purposes of this analysis, the outside surface of the radiator will be called surface 1 and the inside surface 2. It will be assumed that the portion of the MBR surface area that passes through the bath can be neglected as small compared to the full MBR surface. Therefore, an analysis for a full open cylinder will be assumed.

The key parameter required in the analysis is the total view factor of the entire radiator to space, F_{RS}. It is composed of: (1) the view factor of the outer surface to space, F_{1S}, which is always unity; and (2) the view factor of the inner surface to space F_{2S}. The three view factors are related according to the relation:

$$A_B F_{RS} = 0.5 A_B F_{1S} + 0.5 A_B F_{2S} \tag{C.1}$$

where: $A_B = 2A_S$ = inner and outer belt surface area.

Equation (C.1) reduces to:

$$F_{RS} = 0.5 (1 + F_{2S}) \tag{C.2}$$

F_{2S} is calculated by referring to equations previously derived in Reference 2. The view factor F_{34}, of two cylindrical discs (3 and 4) of radius R spaced a distance W apart is given as follows and is illustrated in Figure 21.

$$F_{34} = \frac{1 + 2\left(\frac{R}{W}\right)^2 - \sqrt{1 + 4\left(\frac{R}{W}\right)^2}}{2\left(\frac{R}{W}\right)^2} \tag{C.3}$$

Equation (C.3) is related to the view factor of the inner surface of a cylinder, surface 2, to space (in this case the ends of the cylinder) via the following relationships.

Since it may be proved that:

$$F_{23} = F_{24}$$

the expression:

$$F_{22} = 1 - F_{23} - F_{24}$$

may be rewritten as:

$$F_{22} = 1 - 2F_{23} \tag{C.4}$$

Furthermore, since

$$A_3 F_{32} = A_2 F_{23}$$

and:

$$F_{32} = 1 - F_{34}$$

or we may write:

$$F_{23} = \frac{A_3}{A_2}(1 - F_{34}) \tag{C.5}$$

By substituting Equation (C.5) into (C.4), the useful expression:

$$F_{22} = 1 - 2\left[\frac{A_3}{A_2}(1 - F_{34})\right] \tag{C.6}$$

can be derived. F_{34} is calculated from Equation (C.3).

Finally, the view factor to space of the inner surface of the cylindrical belt array is given by:

$$F_{2S} = 1 - F_{22}$$

$$F_{2S} = 2\left[\frac{A_3}{A_2}(1 - F_{34})\right] \tag{C.7}$$

The calculation of the full MBR view factor to space is completely derived by substituting Equation (C.7) into (C.2) to give:

$$F_{RS} = 0.5 + \frac{A_3}{A_2}(1 - F_{34}) \tag{C.8}$$

The results of a parametric evaluation of Equations (C.6), (C.7), and (C.8) are plotted in Figure 22.

References to Appendix C

(1) Preliminary Evaluation of a Liquid Belt Radiator for Space Applications, NASA Contractor Report 174807, December, 1984.

(2) Jacob, M., Heat Transfer, Vol. II, John Wiley & Sons, New York, 1957.

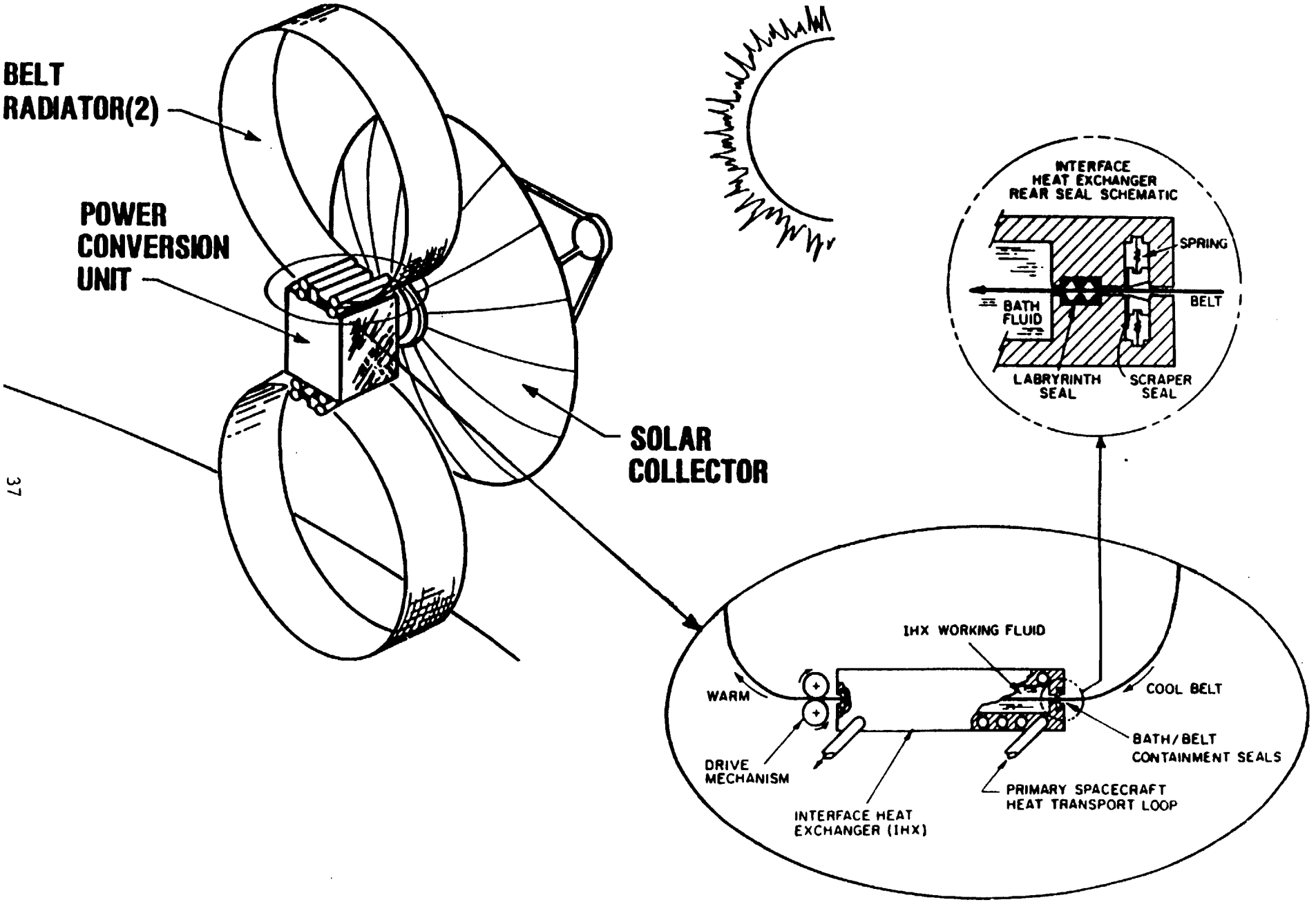

Figure 1 Moving Belt Radiator Concept

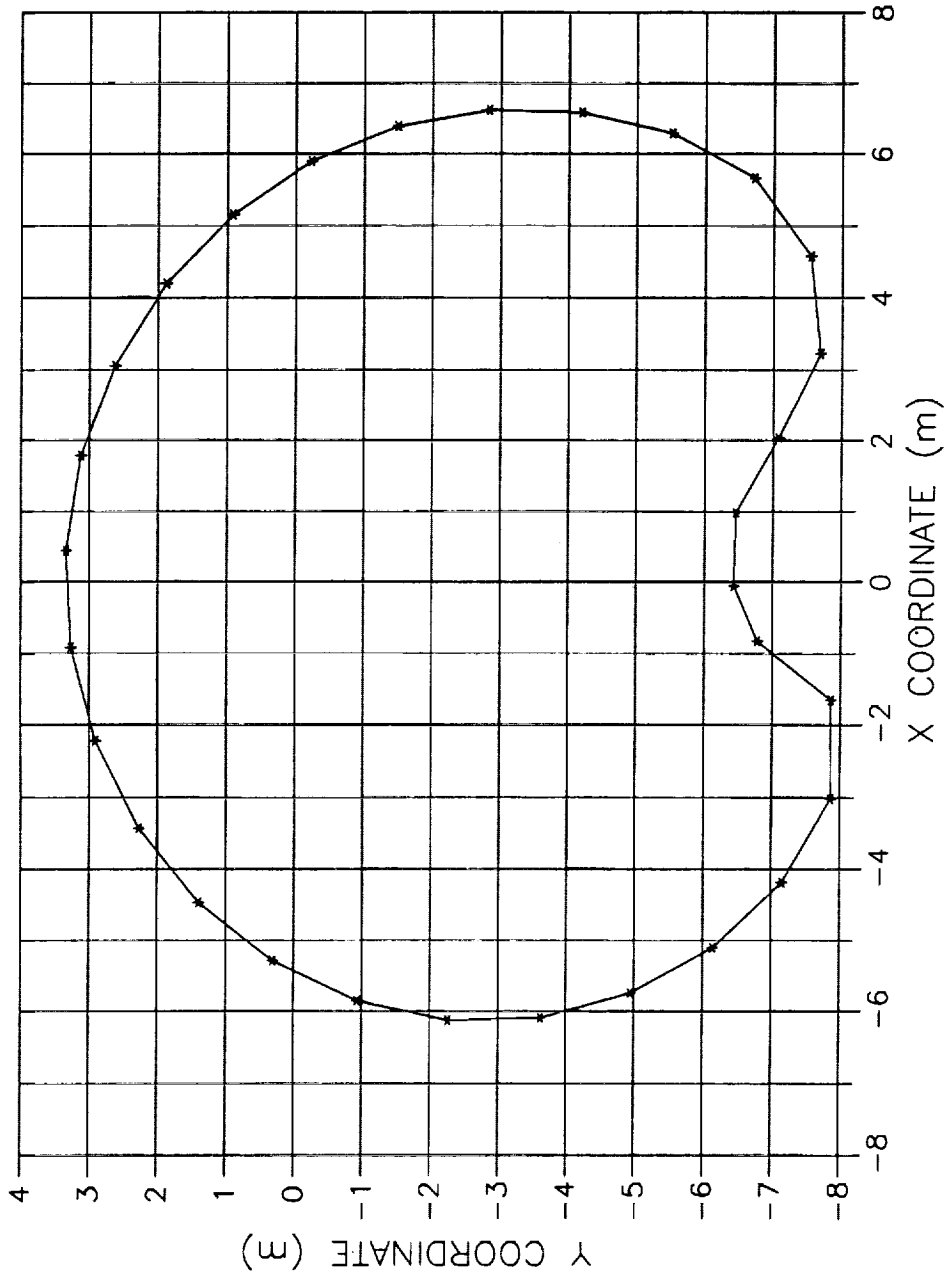

Figure 2 Typical Belt Shape, Plot Generated by BERS (at 3.51 seconds, acceleration: 0.50 m/s/s)

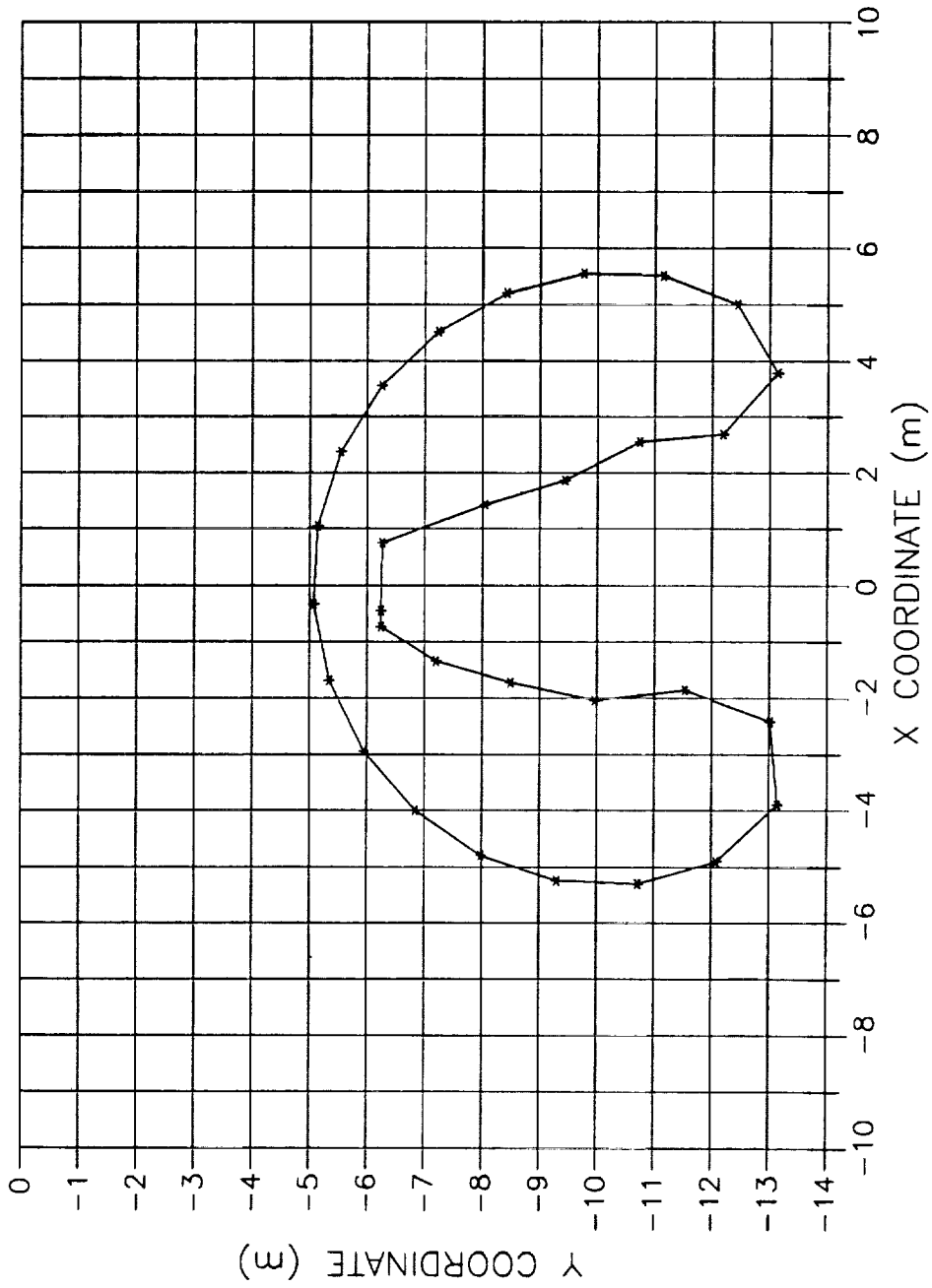

Figure 3 Typical Belt Shape, Plot Generated by BERS (at 1.50 seconds, acceleration: 10.0 m/s/s)

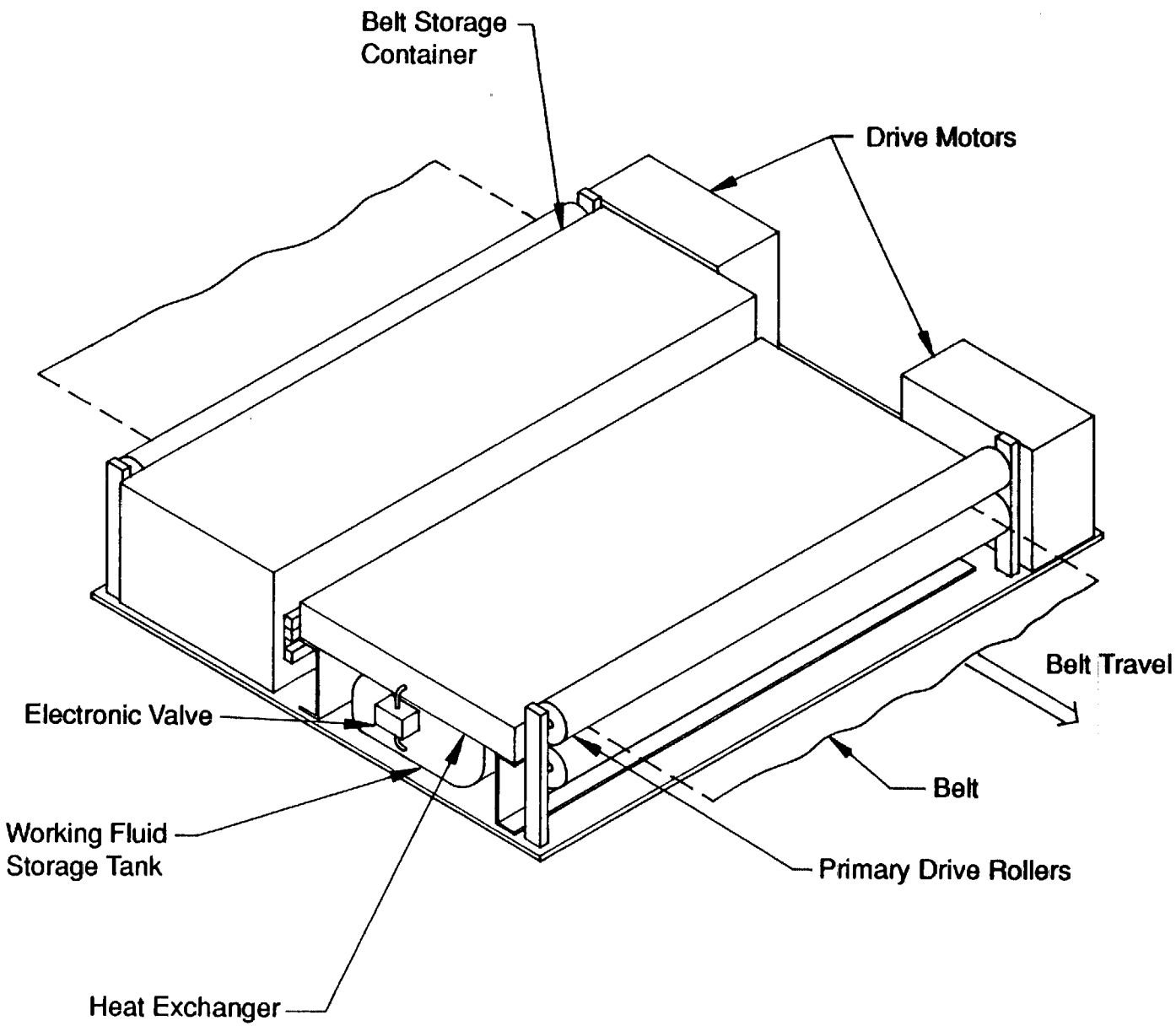

Figure 4 MBR Shuttle Experiment Drive Apparatus

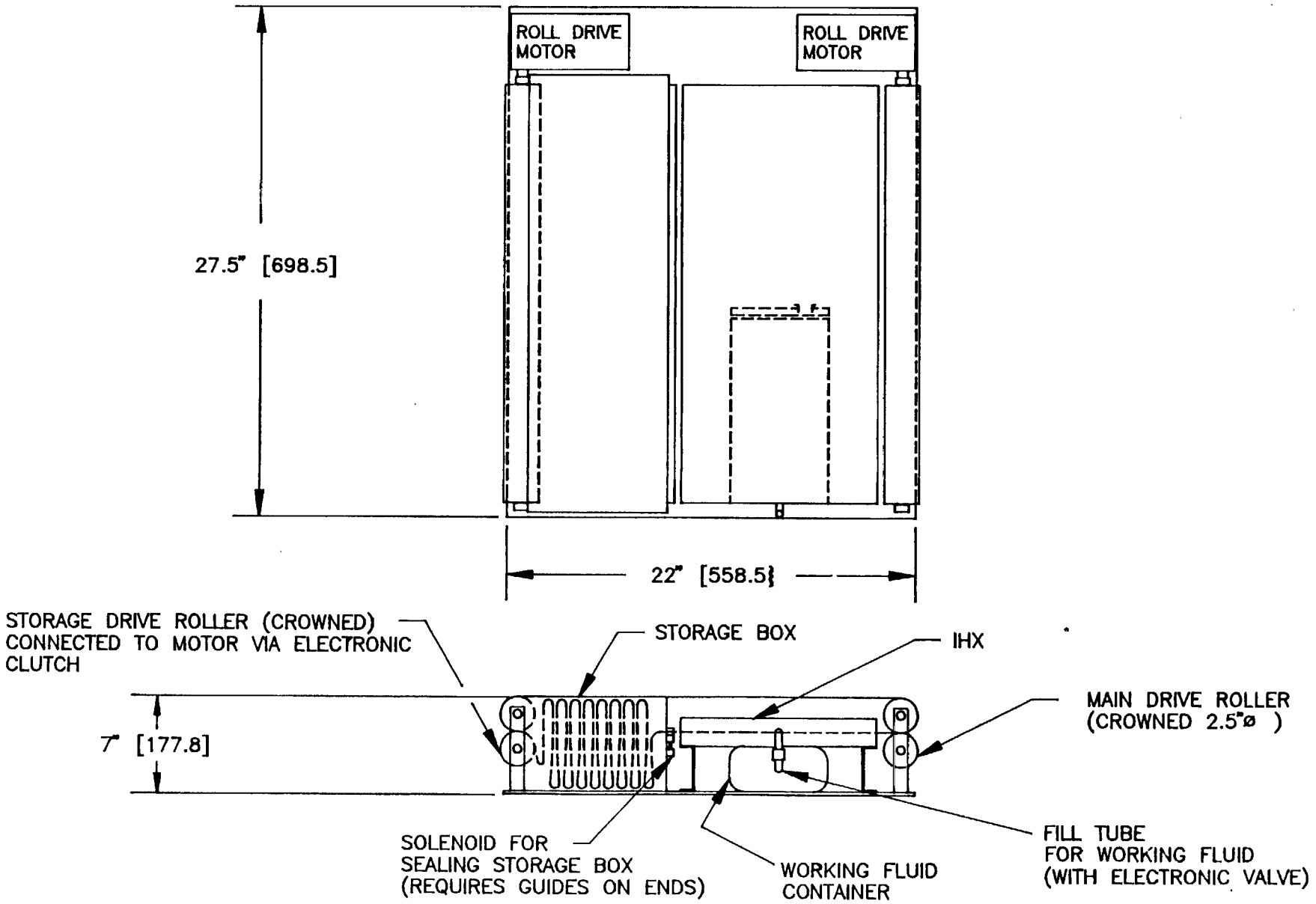

Figure 5 Belt Storage and Drive System Design

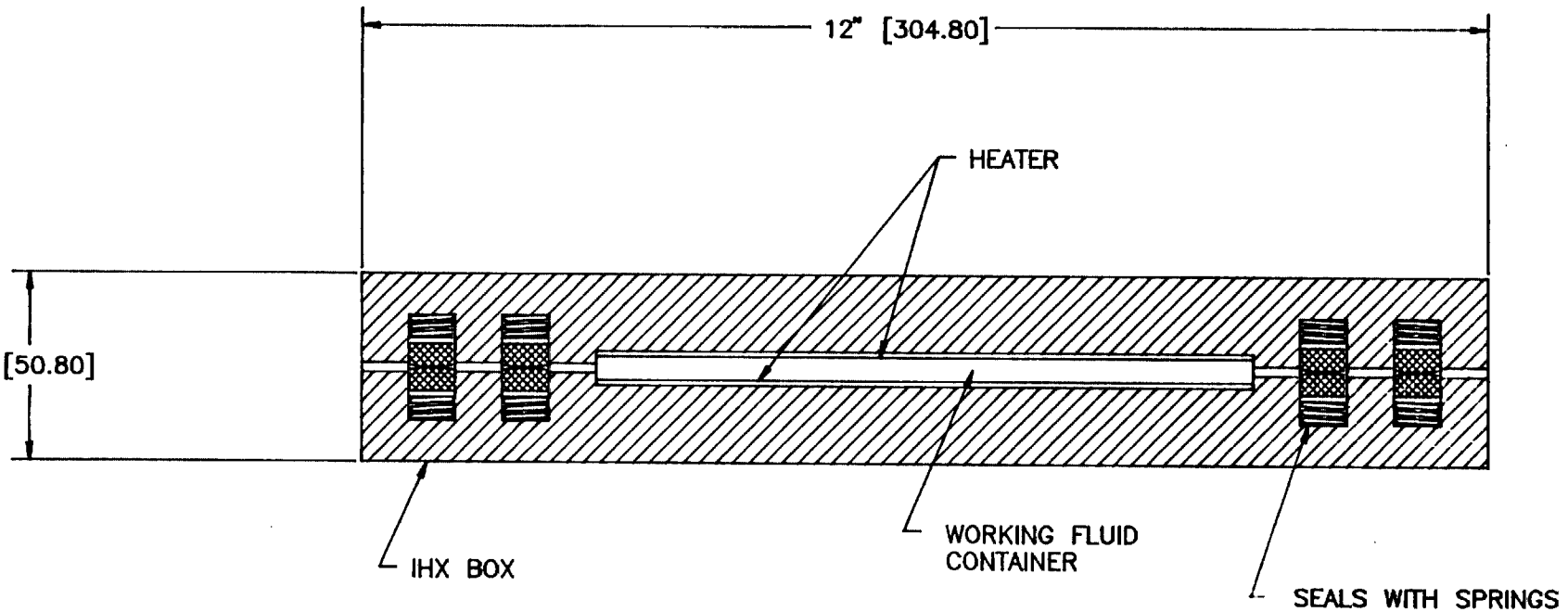

Figure 6A Interface Heat Exchanger Design

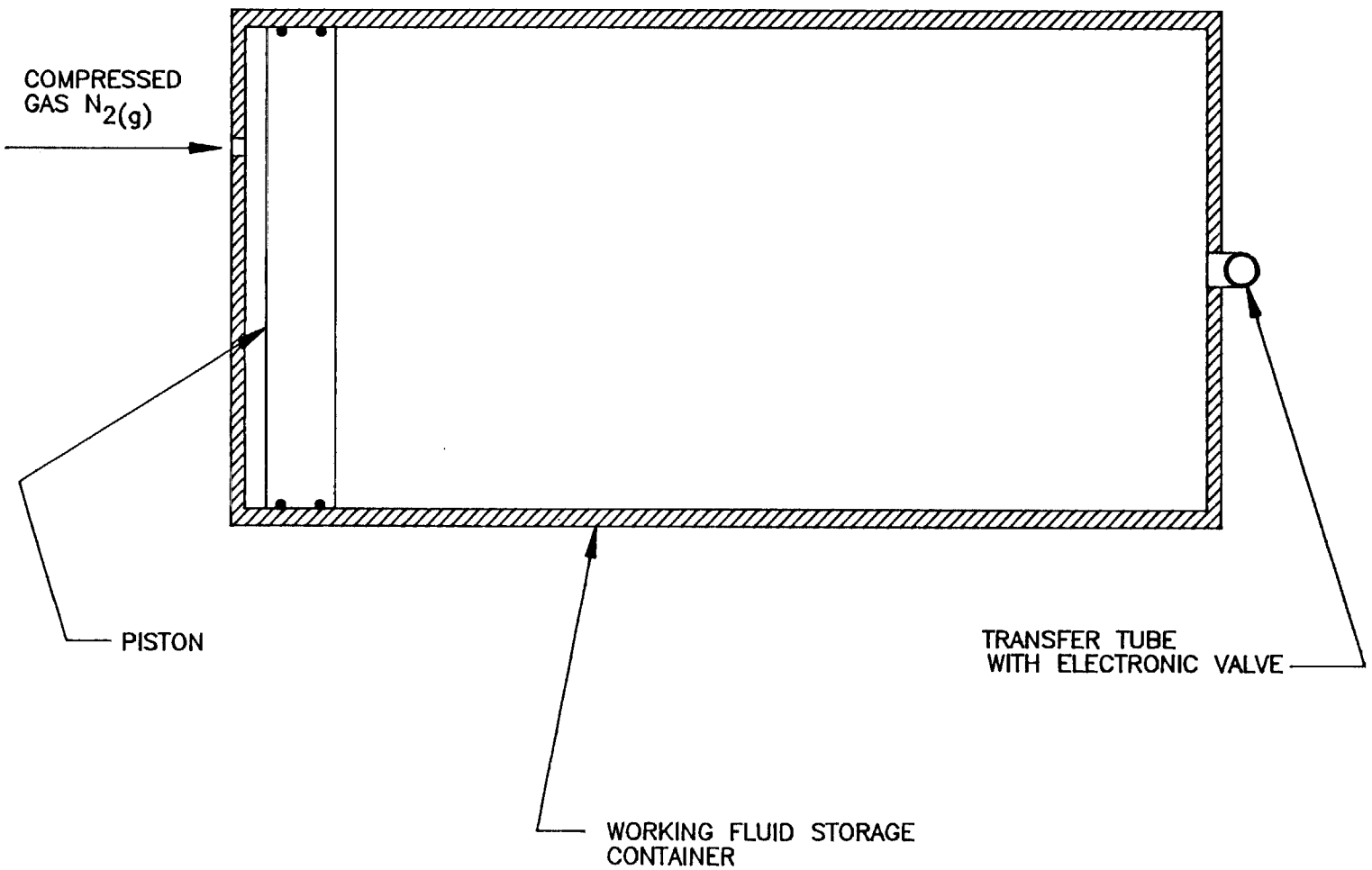

Figure 6B Working Fluid Storage Tank Design

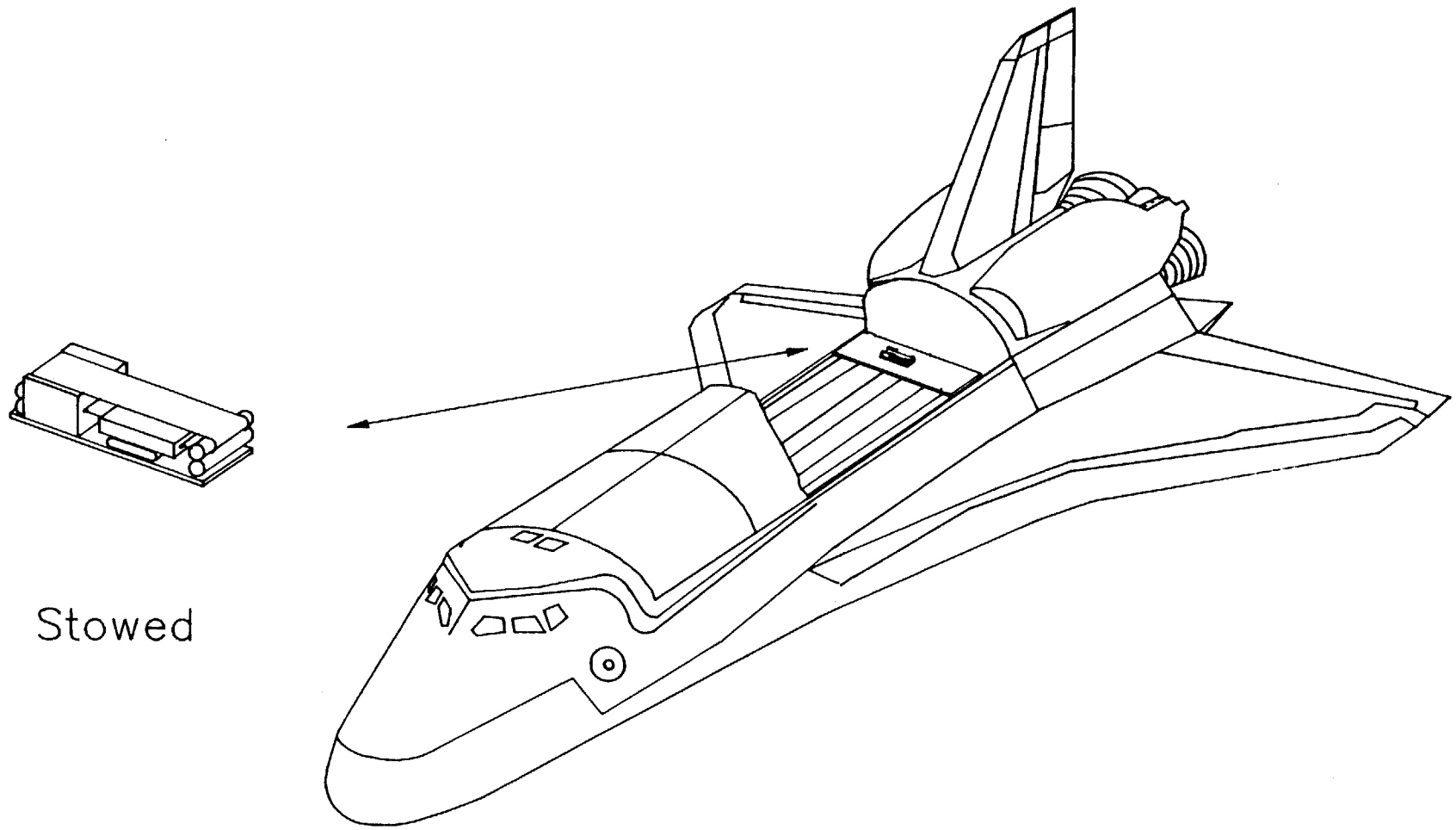

Figure 7 Shuttle with MBR Experiment in Stowed Configuration

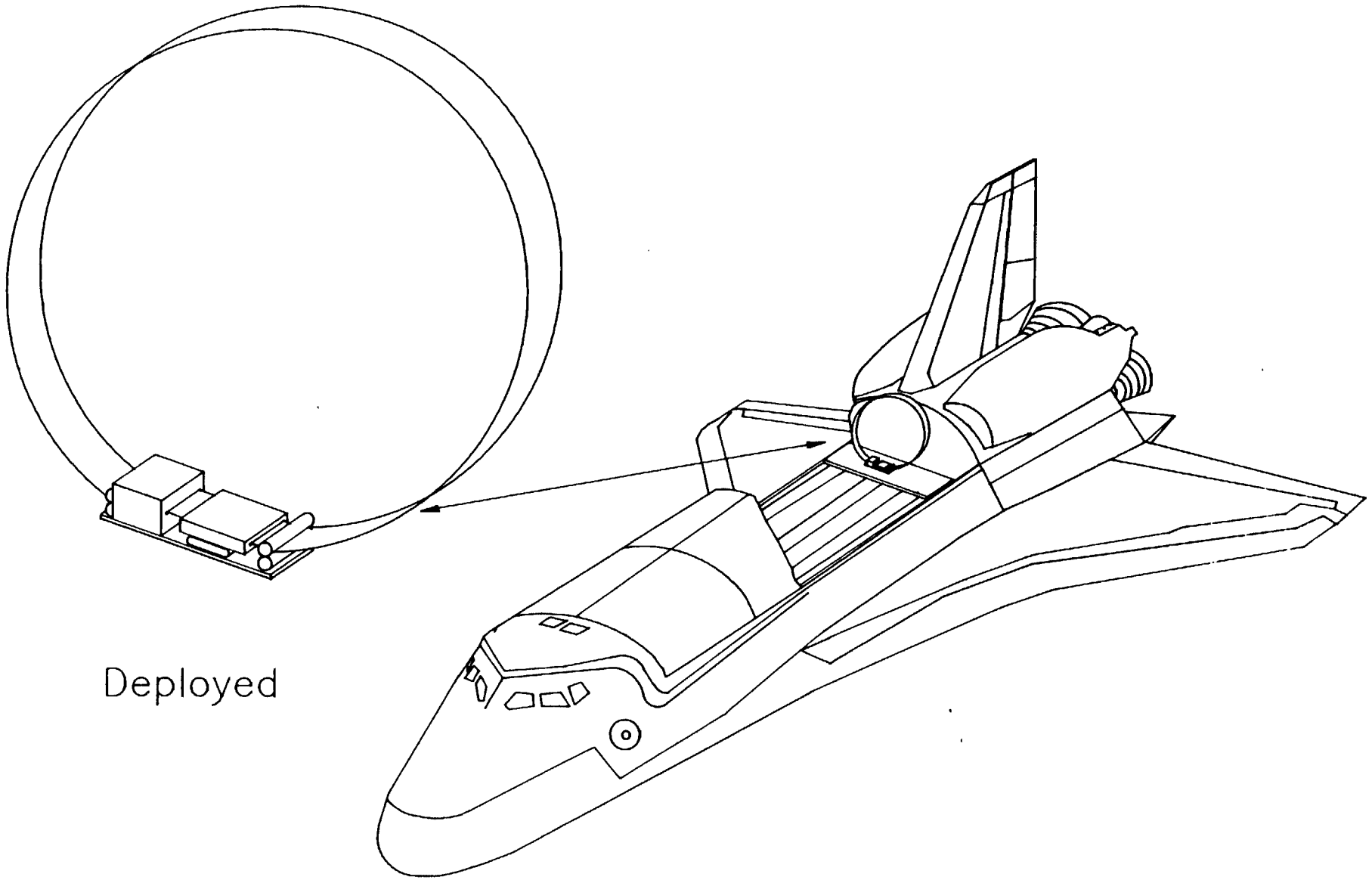

Figure 8 Deployed MBR in Shuttle Bay

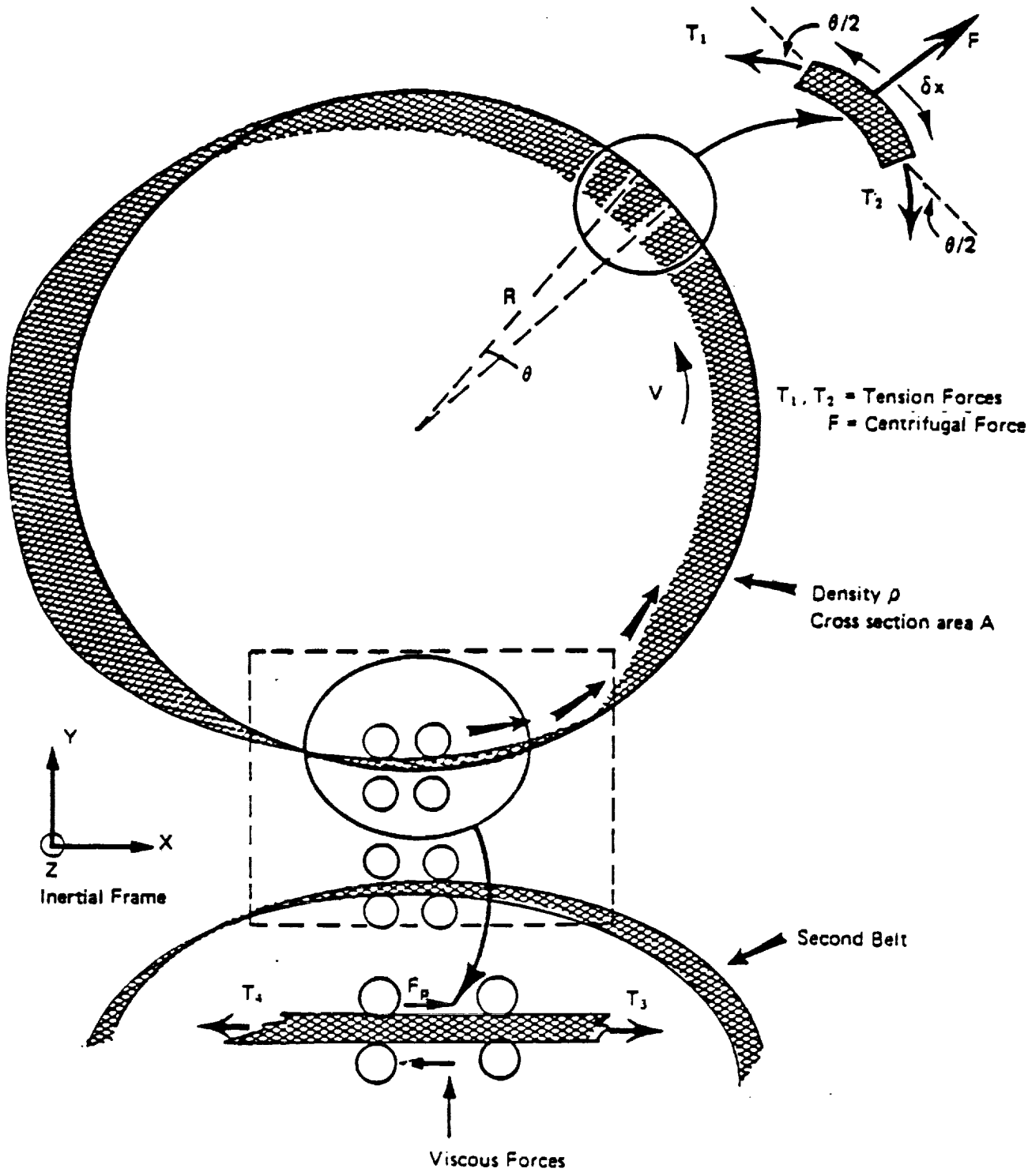

Figure 9 Steady-State Condition of the Belt

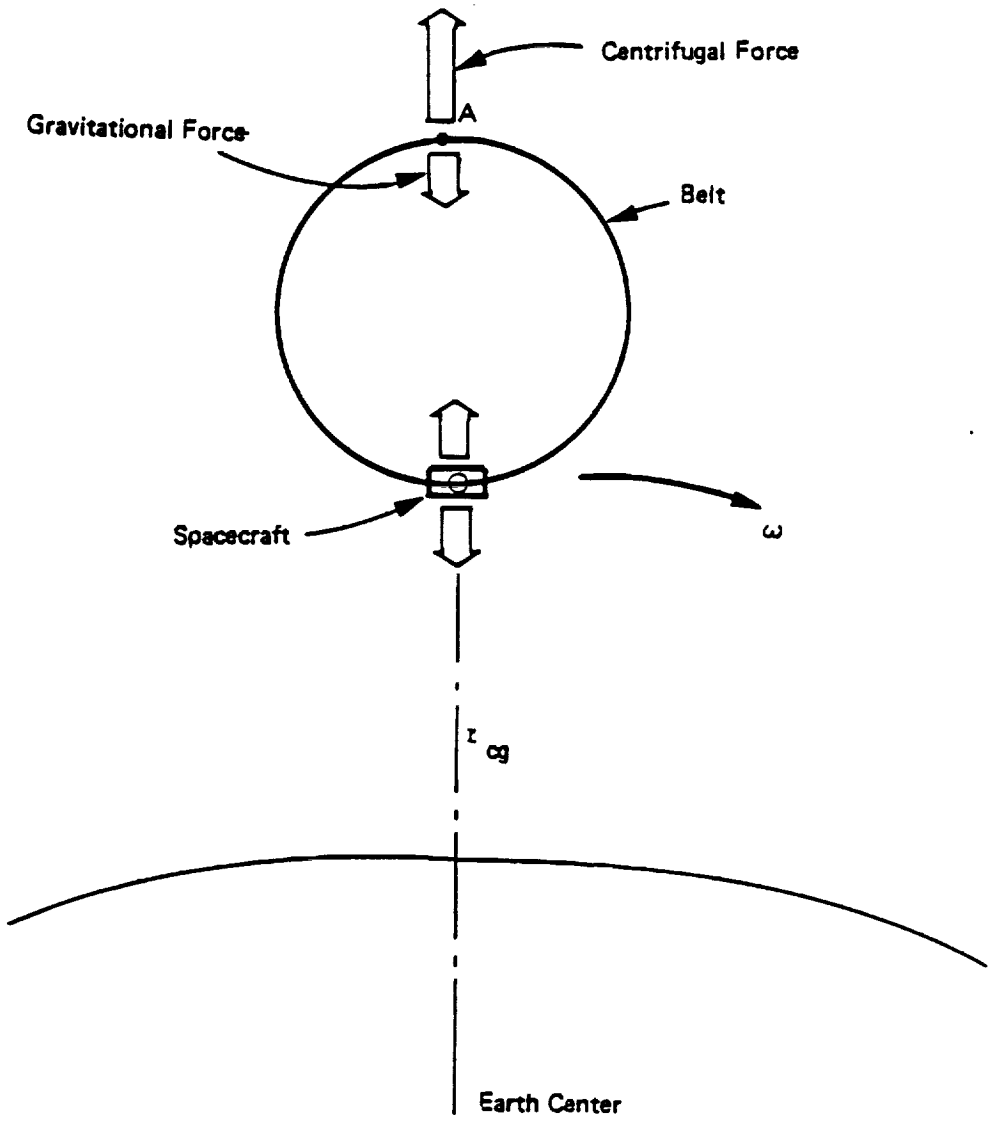

Figure 10 An Imbalance in Centrifugal and Gravitational Forces

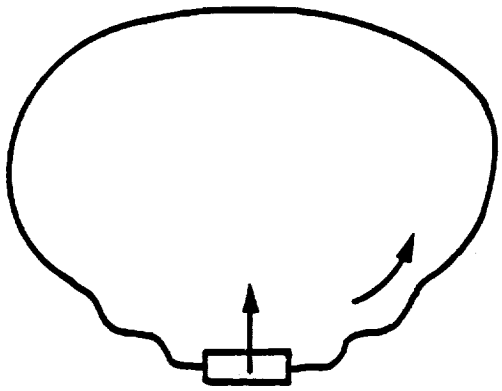

(a) In-plane Bending Vibrations in Belt Due to Small Displacement of Spacecraft Along Y Direction

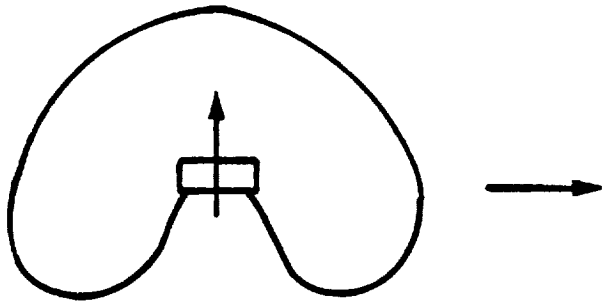

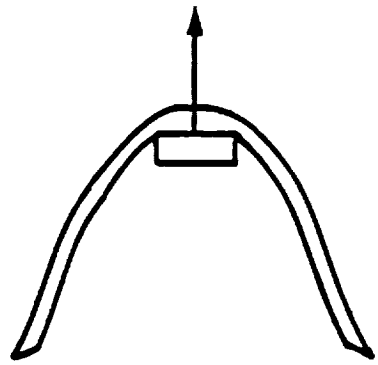

(b) Gross Deformation of Belt Due to Large Displacement of Spacecraft Along Y Direction

(c) Belt Failure

Figure 11 Vibration and Gross Deformation in Belt Due to Y Direction Translation of Spacecraft

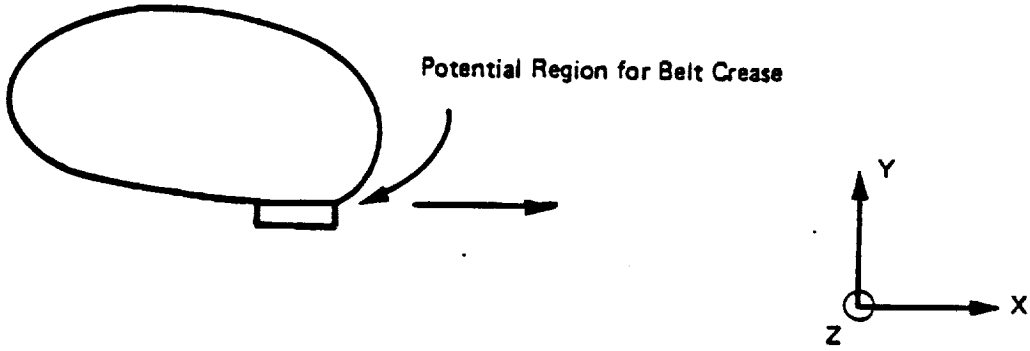

(a) Translation Along X Axis

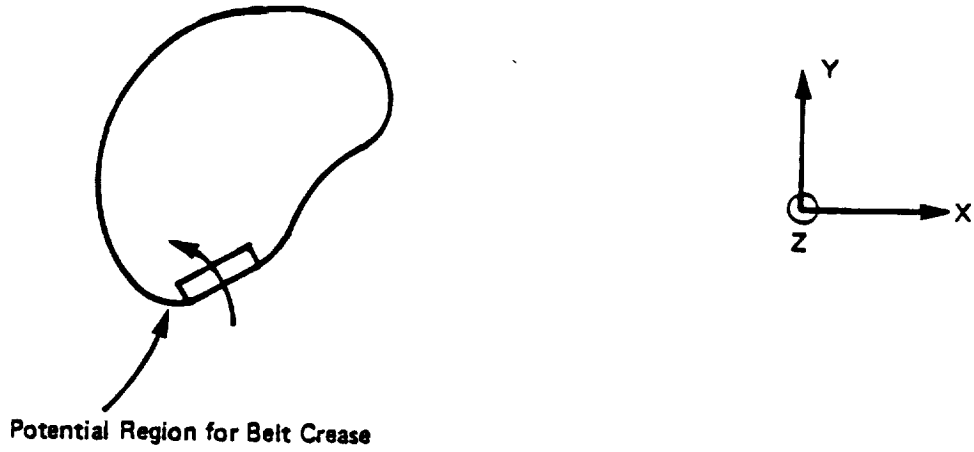

(b) Rotation Around Z Axis

(For translation along Y axis, see Figure 2.3 (b).)

Figure 12 Gross Deformation in Belt Due to In-Plane Motion of Spacecraft

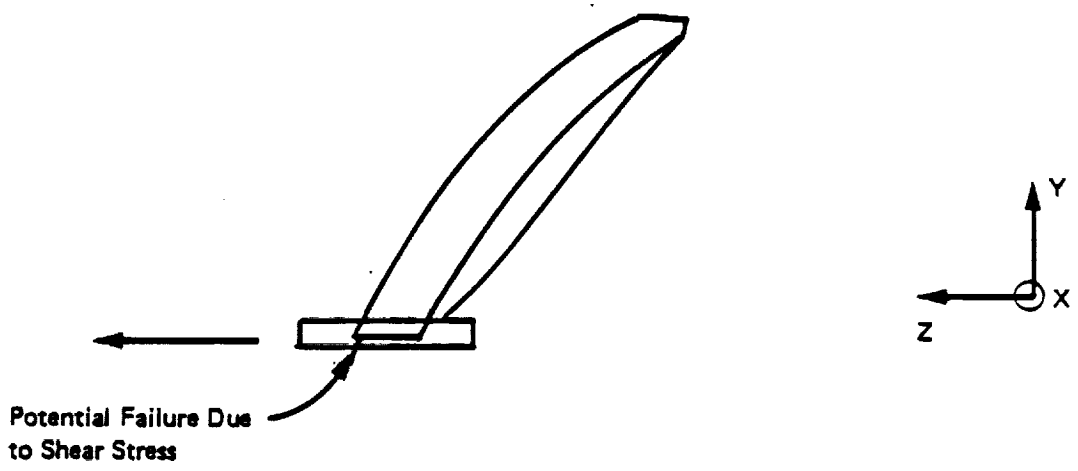

(a) Acceleration Along Z Axis

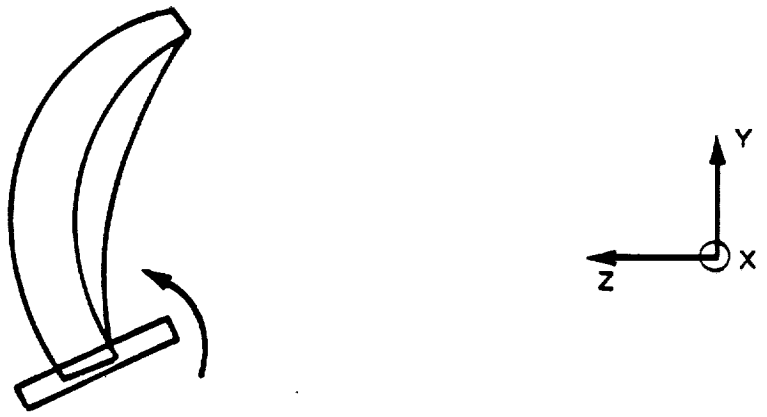

(b) Rotation Along X Axis

Figure 13 Gross Deformation in Belt Due to Out-of-Plane Motion of the Spacecraft

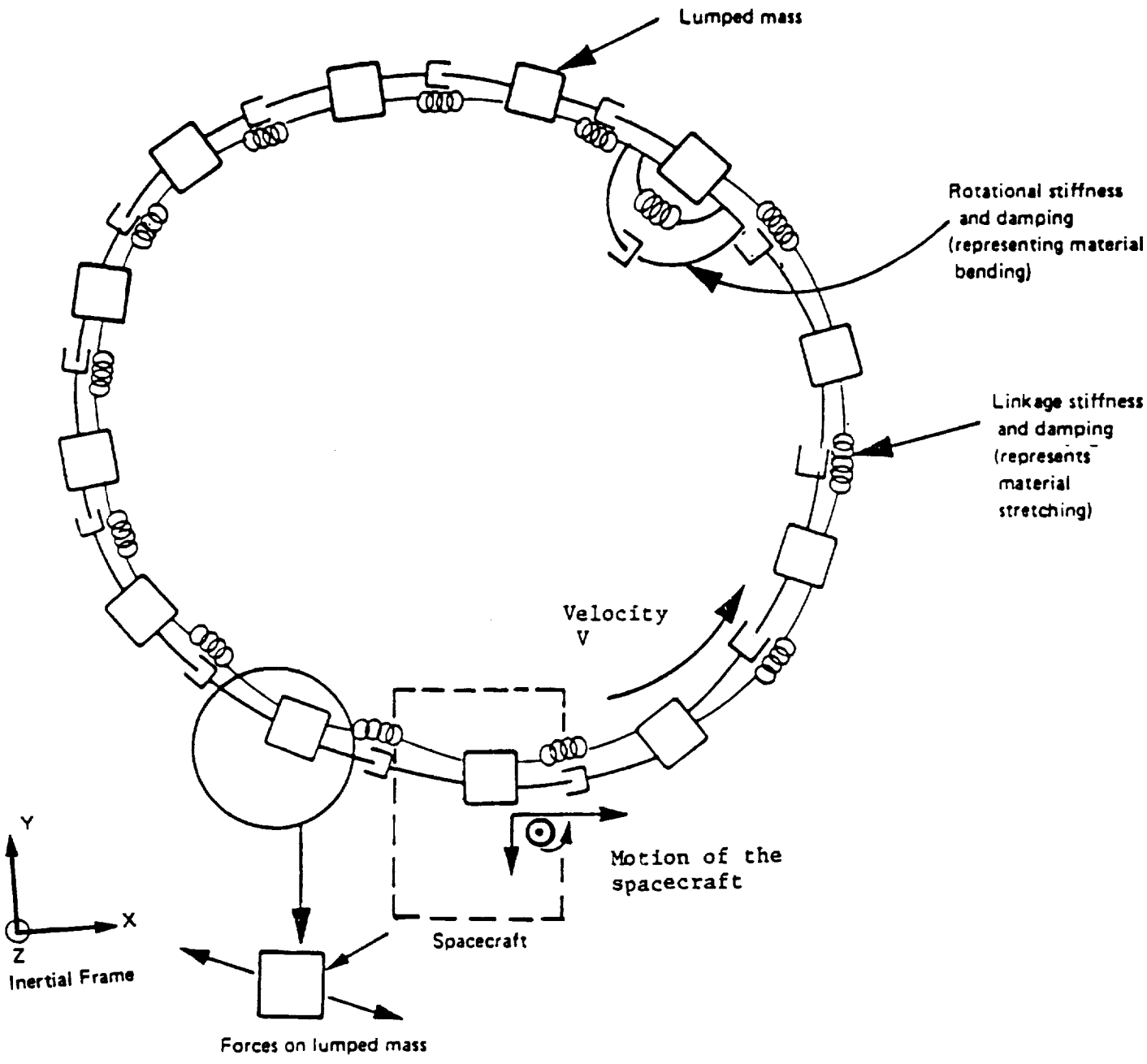

Figure 14 Lumped Parameter Representation of the MBR for Investigation of In-Plane Motion

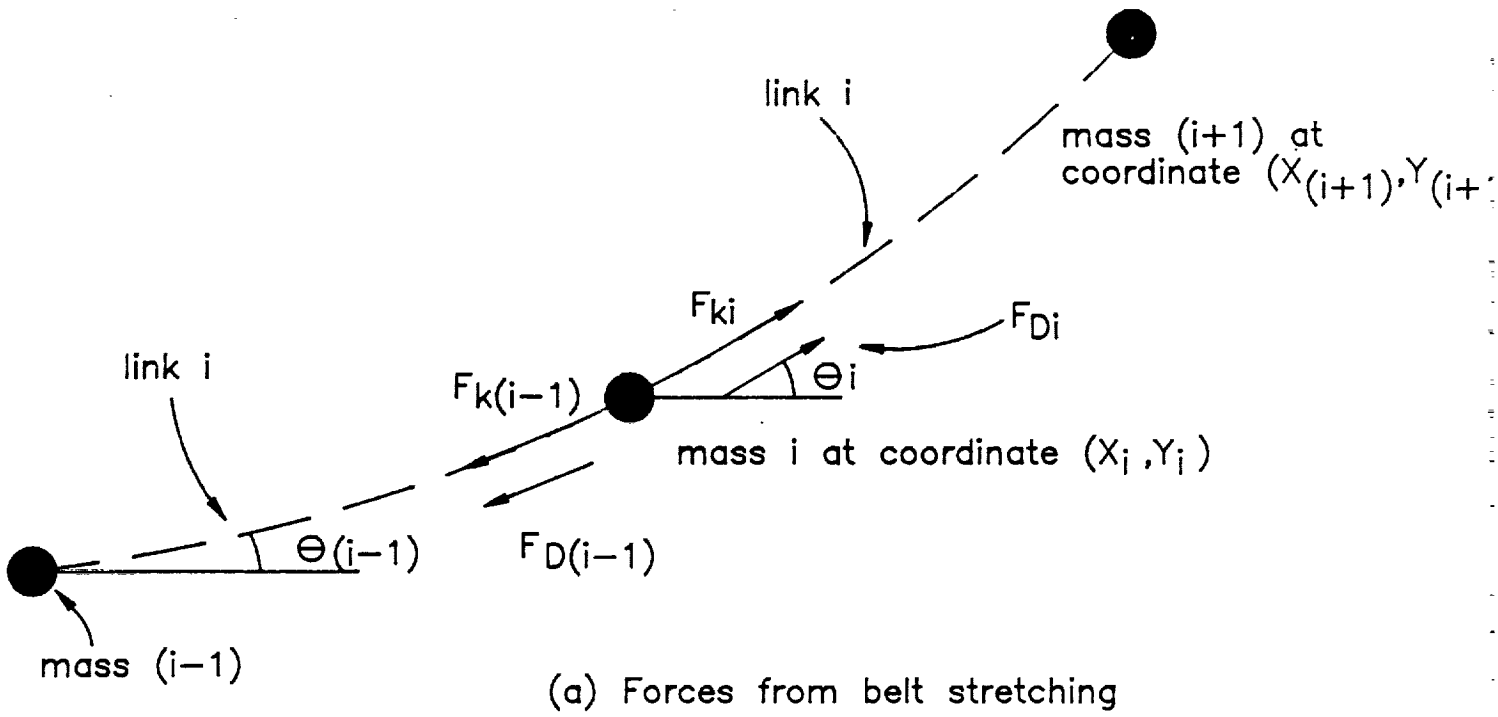

(a) Forces from belt stretching

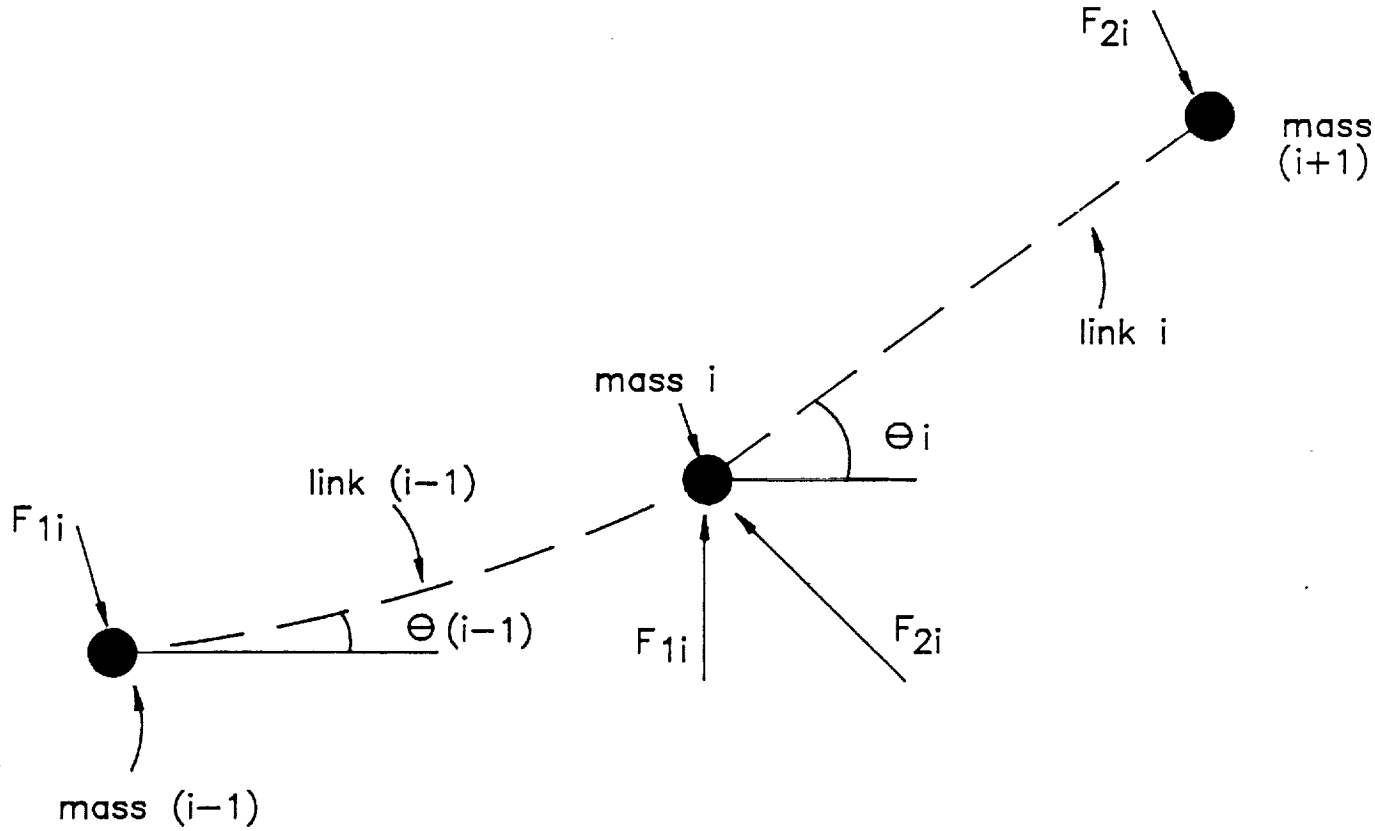

(b) Forces from belt bending

Figure 15 Forces Acting on Lumped Masses

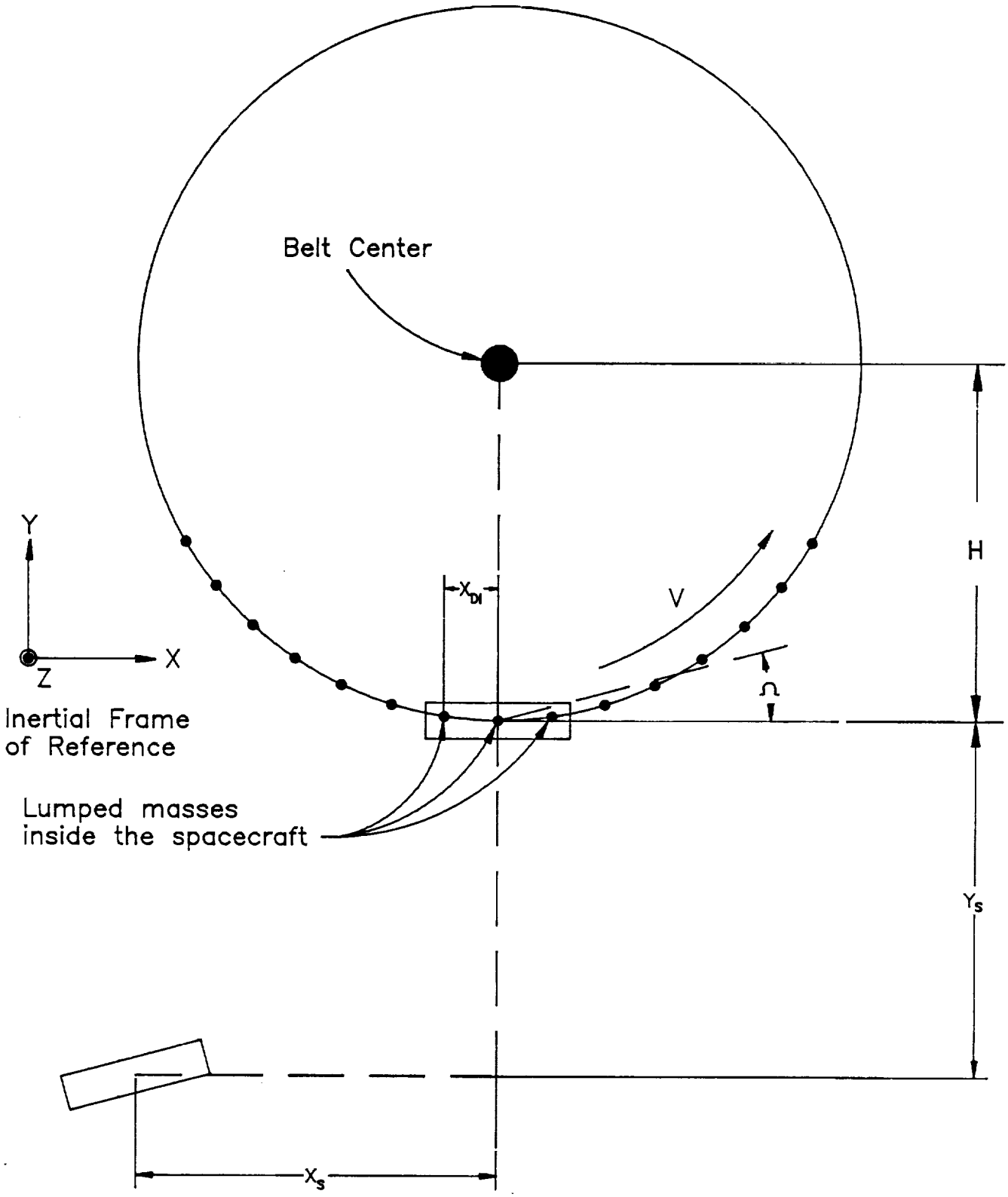

Figure 16 Spacecraft Motion in the Inertial Frame

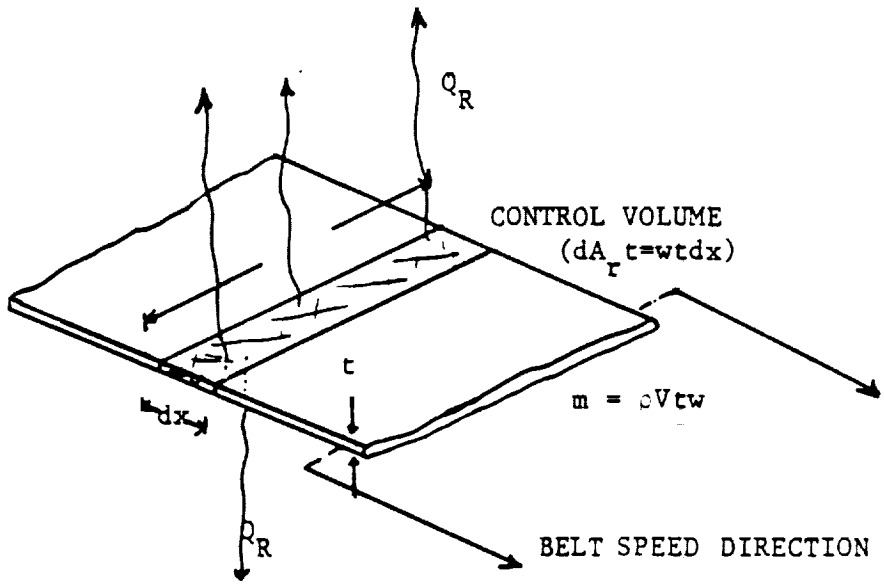

Figure 17 LBR Differential Control Volume

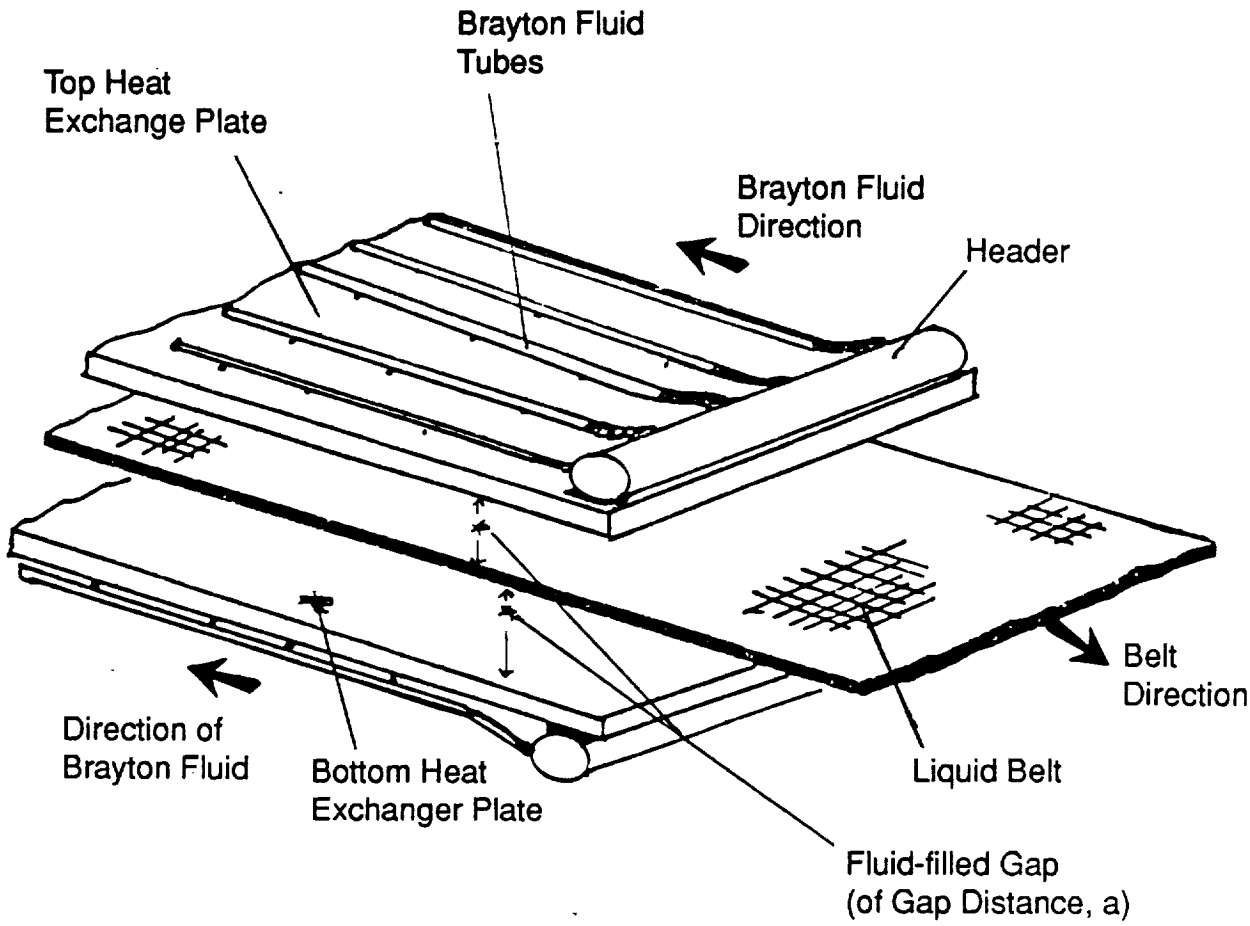

Figure 18 Schematic of Interface Heat Exchanger

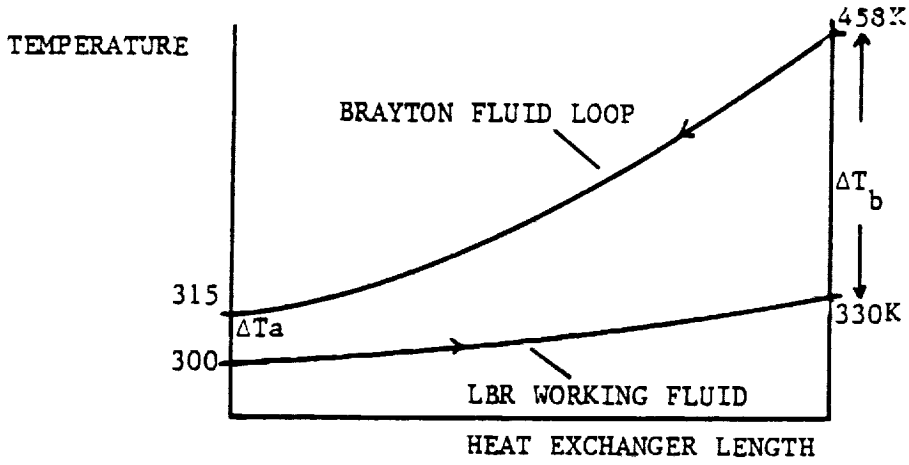

Figure 19 Point Design Interface Heat Exchanger Temperature Differentials for Use in LMTD Calculations (Rohsenow and Choi, p. 310)

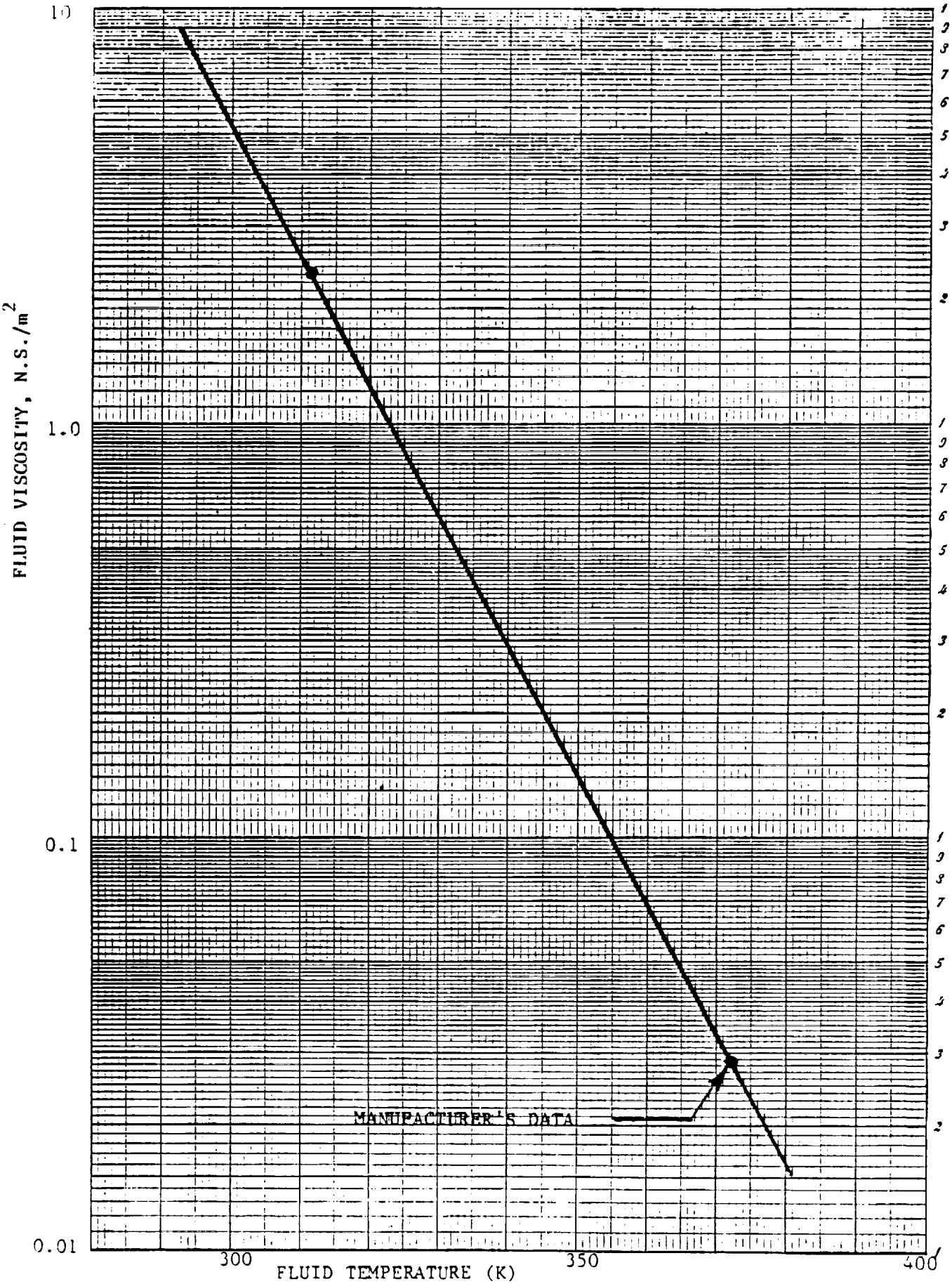

Figure 20 Viscosity of Santovac 6 as a Function of Temperature

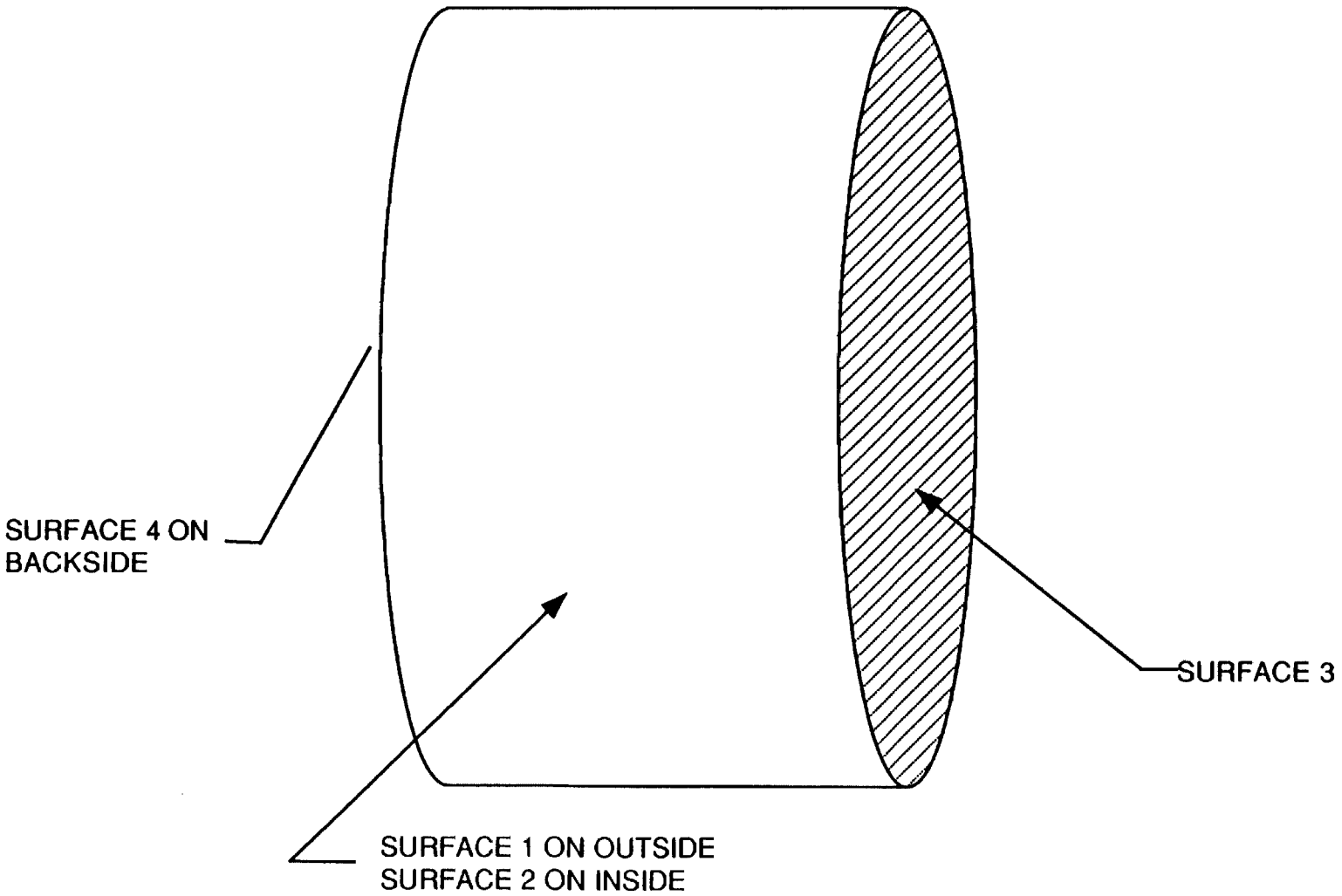

Figure 21 Geometry for View Factor Calculations

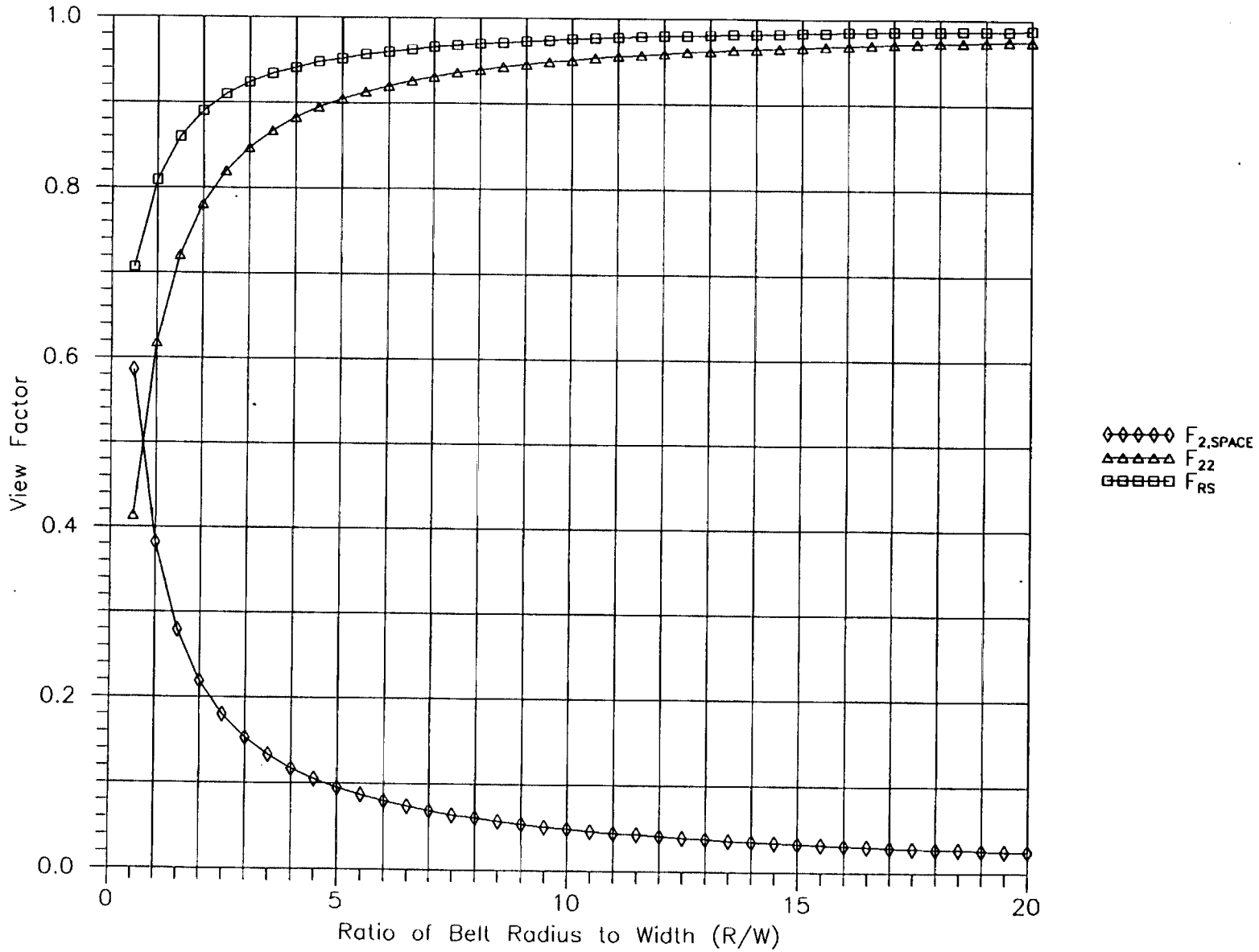

Figure 22 View Factors for Cylindrical LBR Configuration

NASA
National Aeronautics and Space Administration

Report Documentation Page

1. Report No.	2. Government Accession No.	3. Recipient's Catalog No.
NASA CR-185168		

4. Title and Subtitle	5. Report Date
Conceptual Design of MBR Shuttle-Attached Experiment Technical Requirements Document	November 1989
	6. Performing Organization Code

7. Author(s)	8. Performing Organization Report No.
Jerry L. Aguilar	
	10. Work Unit No. 506-48-4A

9. Performing Organization Name and Address	11. Contract or Grant No.
Arthur D. Little, Inc. 20 Acorn Park Cambridge, MA 02140	NAS3-25356
	13. Type of Report and Period Covered
12. Sponsoring Agency Name and Address	Contractor Report Final
NASA Lewis Research Center 21000 Brookpark Road Cleveland, OH 44135	14. Sponsoring Agency Code

15. Supplementary Notes

Project Manager, Alan White, Power Technology Division, NASA Lewis Research Center.
In-Space Experiments Focal Point, Olga Gonzalez-Sanabria

16. Abstract

The technical requirements for a shuttle-attached Moving Belt Radiator (MBR) experiment are defined. The MBR is an advanced radiator concept in which a rotating belt radiates thermal energy to space. The requirements for integrating the MBR experiment in the shuttle bay are discussed. Requirements for the belt material and working fluid are outlined along with some possible options. The proposed size and relationship to a full scale Moving Belt Radiator are defined. The experiment is defined with the primary goal of dynamic testing and a secondary goal of demonstrating the sealing and heat transfer characteristics. A perturbation system which will simulate a docking maneuver or other type of short term acceleration is proposed for inclusion in the experimental apparatus. A deployment and retraction capability which will aid in evaluating the dynamics of a belt during such a maneuver is also described. The proposed test sequence for the experiment is presented. Details of the conceptual design are not presented herein, but rather in a separate Final Report.

17. Key Words (Suggested by Author(s))	18. Distribution Statement
Moving Belt Radiator Advanced Space Radiator Space Power Shuttle Experiment	Unclassified-Unlimited Subject Category 20

19. Security Classif. (of this report)	20. Security Classif. (of this page)	21. No of pages	22. Price*
Unclassified	Unclassified	59	A04

*For sale by the National Technical Information Service, Springfield, Virginia 22161